Optical absorption and Sommerfeld factors of one-dimensional semiconductors: An exact treatment of excitonic effects

Tetsuo Ogawa and Toshihide Takagahara
NTT Basic Research Laboratories, 3-9-11 Midori-cho, Musashino-shi, Tokyo 180, Japan
(Received 6 May 1991)

We investigate theoretically excitonic effects on the optical properties of one-dimensional (1D) semiconductors. In particular, absorption spectra near a band edge are exactly calculated within the effective-mass approximation for the 1D system with a direct allowed or forbidden gap. We employ two kinds of interaction potentials between an electron and a hole describing a modified Coulomb interaction and a short-range interaction, both of which are free from the well-known divergence problem of the 1D Coulomb system. The Sommerfeld factor, which is the absorption intensity ratio of the unbound (continuum) exciton to the free-electron-hole pair above the band edge, is found to be *smaller than unity* for the direct allowed transition, in striking contrast to the 3D and 2D cases. This peculiar feature is interpreted in terms of the anomalously strong concentration of the oscillator strength on the lowest discrete exciton state. On the other hand, for the direct forbidden transition, the Sommerfeld factor in the 1D system is larger than unity and shows similar behavior to those in the 3D and 2D cases. These properties hold irrespective of the interaction range of the electron-hole attractive potential. The feasibility of the model potentials is examined, and the Coulomb potential having a cusp-type cutoff is found to be the most effective to describe the potential in an actual semiconductor wire. A dielectric effect in the wire structure is shown to enhance these peculiar features of the 1D system.

I. INTRODUCTION

Semiconductor nanostructures are attracting much interest not only from the viewpoint of fundamental physics, but also from the expectation of their potential applications to various optical and electronic devices. Quantum confinement in more than one dimension is realized in quantum wires or quantum boxes made of inorganic semiconductor compounds. With quantum wires an interesting optical anisotropy in the photoluminescence excitation spectra[1] and stimulated emission from quantum-wire heterostructures[2] were successfully observed. In these materials low-dimensional effects are well reflected in their optical responses. In turn, the optical properties are good measures to explore the intrinsic nature of low-dimensional systems.

Quantum wires offer a good stage where electrons and holes are free to move in only one spatial dimension. One of the most striking features of the one-dimensional (1D) system is the inverse-square-root divergence of the joint density of states at the energy of the fundamental optical gap, which will be called the "band edge" in this paper. This feature will be manifest most remarkably in optical-absorption spectra. The singularity in the density of states is expected to appear above the band edge, namely, in the interband absorption spectra. Thus it is of great importance to study the linear absorption spectra around the band edge in order to clarify the characteristic features of the 1D system.

In the optical-absorption spectra, excitonic effects play important roles, particularly in low-dimensional systems. In a previous paper,[3] we briefly reported characteristic features of the 1D exciton formed by a long-range Coulomb interaction between an electron and a hole. In this paper we examine more extensively the 1D excitonic effects on the absorption spectra, comparing with three- and two-dimensional cases, and clarify peculiar behaviors of the Sommerfeld factor, which is the absorption intensity ratio of the unbound (continuum) exciton to the free electron-hole pair above the band edge.

The ideal limit of the 1D electron-hole system, namely, infinitesimal wire cross section and perfect confinement, has been treated as a "one-dimensional hydrogen-atom" problem[4] in the framework of the effective-mass theory. Bound states (1D discrete excitons) of this system were studied by Elliott and Loudon[5] who clarified pathological features of the 1D exciton below the band edge, e.g., (i) the divergence of the binding energy of the lowest-energy exciton, (ii) the δ-function-like wave function of the lowest exciton, and (iii) the violation of the nondegeneracy theorem for 1D bound states. Recently, Abe[6] examined numerically the oscillator strength of 1D excitons in Peierls systems and found a concentration of oscillator strength on the lowest exciton state. Thus the lowest bound state in the 1D system was found to show singular characteristics. Unlike for the bound states, there are few studies on unbound (continuum) states of a 1D electron-hole pair, which contribute directly to the interband absorption. It has not yet been clarified how the anomalies of the lowest bound state affect the interband absorption. The interplay between effects of the 1D excitonic absorption due to the bound states and of the diver-

 ©1991 The American Physical Society

gence of the 1D joint density of states is to be investigated in discussing the continuum absorption above the band edge. This is a main purpose of this paper. Because there exist well-known singular characteristics in the 1D Coulomb system, it is desirable to study the system rigorously without the use of approximation tools, e.g., variational methods and WKB methods, to avoid ambiguities.[7] Therefore, we shall study exactly solvable models for an electron-hole pair confined in a purely one-dimensional system with a modified Coulomb interaction or other model potentials.

The second purpose of this paper is to clarify comprehensively characteristic features of the oscillator strength of the discrete bound states of the 1D exciton. In particular, we focus our attention on the concentration of the oscillator strength on the lowest bound state and also on the dependence of the degree of concentration upon the potential shape. This study provides a key idea to understand peculiar behaviors of the interband absorption of the 1D system.

This paper is organized as follows. In Sec. II three attractive potentials between an electron and a hole are introduced to make our model analytically solvable without the divergence difficulty. Two of them are slight modifications of the long-range Coulomb potential in which a cusp-type cutoff is employed, and the other one represents a short-range interaction. Therefore, we can compare effects of the interaction range on optical properties. In Sec. III we solve exactly the 1D Schrödinger equation for the above potentials within the effective-mass approximation and obtain normalized wave functions of the unbound state. Interband absorption coefficients for both allowed and forbidden transitions and corresponding Sommerfeld factors are analytically calculated with the use of the unbound wave functions. Properties of discrete bound states of the 1D exciton are clarified in Sec. IV to reveal their characteristic features which come essentially from the one dimensionality. Comparisons with the 3D and 2D cases are made in Sec. V. The feasibility of the model potentials employed in this paper and a dielectric effect on the electron-hole attractive potential are also discussed there.

II. ATTRACTIVE INTERACTIONS BETWEEN AN ELECTRON AND A HOLE

To calculate the energy spectra of excitons and their optical properties, we must solve the Schrödinger equation. In the effective-mass and envelope-function approximations, this equation is given as

$$\left[-\frac{\hbar^2}{2m_e}\nabla_e^2-\frac{\hbar^2}{2m_h}\nabla_h^2+U_e(r_e)+U_h(r_h)+V(r_e,r_h)\right]\times\Phi(r_e,r_h)=\tilde{E}\Phi(r_e,r_h)\ , \quad (2.1)$$

where m_e (m_h) is the effective mass of an electron (a hole), U_e (U_h) is the confinement potential for the electron (hole), and V is the electron-hole Coulomb interaction potential. Here the origin of the eigenenergy $\tilde{E}$ is chosen to be the bulk band-gap energy E_g^{bulk}. In the following we choose the z axis to be the direction of the quantum wire and the x and y axes to be the lateral directions. If the confinement of carriers in the lateral directions is strong enough, the exciton envelope function can be approximated as

$$\Phi(r_e,r_h)=e^{iKZ}f_e^0(x_e,y_e)f_h^0(x_h,y_h)\phi(r_e-r_h)\ , \quad (2.2)$$

where the Cartesian coordinates of the electron (hole) are denoted with the suffix e (h), Z (K) is the z coordinate (the wave number) of the center of mass of the exciton, the first factor represents the plane-wave-like motion along the z axis of the exciton center of mass, f_e^0 (f_h^0) is the lowest subband function confined in the lateral directions for the electron (hole), and ϕ is the envelope function describing the electron-hole relative motion. Assuming that ϕ is a function of only z_e-z_h and noting that the subband functions satisfy the equations

$$\left[-\frac{\hbar^2}{2m_e}\left[\frac{\partial^2}{\partial x_e^2}+\frac{\partial^2}{\partial y_e^2}\right]+U_e(x_e,y_e)\right]f_e^0(x_e,y_e)=\varepsilon_e^0 f_e^0(x_e,y_e)\ , \quad (2.3a)$$

$$\left[-\frac{\hbar^2}{2m_h}\left[\frac{\partial^2}{\partial x_h^2}+\frac{\partial^2}{\partial y_h^2}\right]+U_h(x_h,y_h)\right]f_h^0(x_h,y_h)=\varepsilon_h^0 f_h^0(x_h,y_h)\ , \quad (2.3b)$$

where ε_e^0 and ε_h^0 are the subband quantization energies, we can reduce Eq. (2.1) as

$$\left[-\frac{\hbar^2}{2\mu}\frac{\partial^2}{\partial z^2}+V(r_e,r_h)\right]f_e^0(x_e,y_e)f_h^0(x_h,y_h)\phi(z)=\left[\tilde{E}-\varepsilon_e^0-\varepsilon_h^0-\frac{\hbar^2K^2}{2(m_e+m_h)}\right]\times f_e^0(x_e,y_e)f_h^0(x_h,y_h)\phi(z)\ , \quad (2.4)$$

where μ is the electron-hole reduced mass and $z=z_e-z_h$. If $f_e^0$and f_h^0 are normalized as

$$\int dx_e dy_e |f_e^0(x_e,y_e)|^2=1\ , \quad (2.5a)$$

$$\int dx_h dy_h |f_h^0(x_h,y_h)|^2=1\ , \quad (2.5b)$$

Eq. (2.4) is further reduced to

$$\left[-\frac{\hbar^2}{2\mu}\frac{d^2}{dz^2}+V_{\text{eff}}(z)\right]\phi(z)=E\phi(z)\ , \quad (2.6)$$

with

$$E\equiv\tilde{E}-\varepsilon_e^0-\varepsilon_h^0-\frac{\hbar^2K^2}{2(m_e+m_h)}\ , \quad (2.7a)$$

$$V_{\text{eff}}(z)\equiv\int dx_e dy_e dx_h dy_h V(r_e,r_h)\times|f_e^0(x_e,y_e)|^2|f_h^0(x_h,y_h)|^2\ . \quad (2.7b)$$

In this final form, the exciton problem is reduced to a completely one-dimensional equation concerning the z coordinate of the electron-hole relative motion. This is a consequence of the strong confinement in the lateral directions and the assumption that the electron-hole rela-

tive motion can be regarded as purely one dimensional.[8] In a general situation where these assumptions cannot be postulated, the subband mixing and three-dimensional character of the electron-hole relative motion should be taken into account and the exciton problem becomes quite involved. Here, in order to see the essential features of the 1D system, we consider the simplest case and discuss Eq. (2.6) in detail.

The effective attractive potential between an electron and a hole given by Eq. (2.7b) is free from the singularity of the bare Coulomb potential at the origin as a result of averaging with the lateral subband wave functions. However, this effective potential can be given only numerically and the eigenvalue problem of Eq. (2.6) cannot be solved analytically in general. In this paper, as examples of an attractive potential that does not have the singularity at the origin and that also allows fully analytical treatment of Eq. (2.6), we employ the following potentials for $V_{\rm eff}(z)$:

$$V_{\rm long}(z)\equiv -\frac{e^2}{\epsilon_1(|z|+z_0)} , \tag{2.8a}$$

$$V^A_{\rm long}(z)\equiv -\frac{e^2}{\epsilon_1(|z|+z_0)}+\frac{Az_0e^2}{\epsilon_1(|z|+z_0)^2} , \tag{2.8b}$$

$$V_{\rm short}(z)\equiv -V_0{\rm sech}^2\left[\frac{z}{\zeta}\right] , \tag{2.8c}$$

where ϵ_1 is the dielectric constant of the wire material. These potentials are not hypothetical, but have some practical relevance. In fact, the effective potential of Eq. (2.7b) can be fairly well approximated by $V_{\rm long}(z)$ as will be shown in Sec. V. Our main attention will be paid to $V_{\rm long}(z)$ and $V_{\rm short}(z)$. The $V_{\rm long}(z)$ potential describes a *long-range* interaction with a cusp-type cutoff which is characterized by one parameter $z_0\geq 0$. As z_0 decreases, this potential approaches the bare Coulomb one. On the other hand, the $V_{\rm short}(z)$ is a *short-range* interaction specified by the strength V_0 (depth of the potential) and the effective interaction length ζ (width of the potential). This potential may simulate a kind of screening effect under strong excitation. The potential $V^A_{\rm long}(z)$ in Eq. (2.8b) is a modified form of $V_{\rm long}(z)$ and was introduced by Elliott and Loudon[5] to describe the 1D exciton motion under a magnetic field. Although results in this case are similar to those for $V_{\rm long}(z)$, the calculational procedure is easier and simpler than that in the $V_{\rm long}(z)$ case.

III. UNBOUND WAVE FUNCTIONS AND INTERBAND ABSORPTION SPECTRA

A. Long-range interaction cases

1. *Coulomb potential with a cusp-type cutoff $V_{long}(z)$*

In the calculation of the interband transition, the wave functions of the unbound electron-hole pair are necessary. The energy of the interband transition has a continuous spectrum and is positive ($E>0$); it is scaled by a wave number k as $E\equiv\hbar^2k^2/2\mu$. It should be kept in mind that this energy E is related only to the electron-hole relative motion and does not include the bulk band-gap energy $E_g^{\rm bulk}$, the subband quantization energies ε_e^0 and ε_h^0, or the energy of the center-of-mass motion $\hbar^2K^2/2(m_e+m_h)$, as can be seen from Eq. (2.7a). Introducing an independent variable $x\equiv 2ik(|z|+z_0)$ (x is purely imaginary), the 1D Schrödinger equation is reduced to the Whittaker equation, i.e.,

$$\frac{d^2\phi(x)}{dx^2}-\left[\frac{1}{4}+\frac{i\alpha}{x}\right]\phi=0 , \tag{3.1}$$

where

$$\alpha=\frac{1}{a_B^*k} , \tag{3.2}$$

with the bulk exciton Bohr radius $a_B^*\equiv\epsilon_1\hbar^2/\mu e^2$. Two independent solutions of Eq. (3.1) are given as

$$W^{(1)}_{-i\alpha,1/2}(x)\equiv\Gamma(1+i\alpha)xe^{-x/2}\times[F(1+i\alpha,2;x)+G(1+i\alpha,2;x)] , \tag{3.3a}$$

$$W^{(2)}_{-i\alpha,1/2}(x)\equiv\Gamma(1-i\alpha)xe^{-x/2}\times[F(1+i\alpha,2;x)-G(1+i\alpha,2;x)] , \tag{3.3b}$$

where $\Gamma(x)$ is the gamma function and $F(1+i\alpha,2;x)$ and $G(1+i\alpha,2;x)$ are two basis solutions of the confluent hypergeometric equation

$$x\frac{d^2u}{dx^2}+(2-x)\frac{du}{dx}-(1+i\alpha)u=0 . \tag{3.4}$$

Their explicit forms are written down as

$$F(1+i\alpha,2;x)=\sum_{n=0}^{\infty}\frac{(1+i\alpha)_n}{(2)_n}\frac{x^n}{n!} , \tag{3.5a}$$

$$G(1+i\alpha,2;x)=\frac{1}{2\pi i}(e^{-2\pi\alpha}-1)\left[[2\ln x+\pi\cot(\pi+i\pi\alpha)-i\pi]F(1+i\alpha,2;x)-2\sum_{n=0}^{\infty}[\psi(1+n)+\psi(2+n)-\psi(1+n+i\alpha)]\frac{(1+i\alpha)_n}{(2)_n}\frac{x^n}{n!}\right]+\frac{2e^{-\pi\alpha}}{x|\Gamma(1+i\alpha)|^2} , \tag{3.5b}$$

where $(a)_n \equiv \Gamma(a+n)/\Gamma(a)$ with $(a)_0=1$ and $\psi(x) \equiv d \ln\Gamma(x)/dx$ is the digamma function. In the following, Eqs. (3.3) are abbreviated as $W^{(1)}(x)$ and $W^{(2)}(x)$, respectively.

Corresponding to the twofold degeneracy of a state in the continuous energy spectrum, there are two wave functions with different parities,[5] i.e., "gerade" and "ungerade." The derivative of the gerade wave function at the origin vanishes, while the ungerade wave function itself becomes zero at the origin ($z=0$), i.e.,

$$\left.\frac{d}{dx}\phi_k^g(z)\right|_{z=0}=0 \quad \text{for gerade} , \tag{3.6a}$$

$$\phi_k^u(0)=0 \quad \text{for ungerade} . \tag{3.6b}$$

Because our model potential in Eq. (2.8a) is symmetric with respect to the origin, these two functions form a basis set of the problem. Only the gerade component yields an optically allowed transition, while the ungerade component corresponds to the forbidden one.

Normalization of the wave function of a continuous state is an important procedure in calculating the absorption intensity because the value of the wave function at the origin ($z=0$) is reflected directly in the intensity. We employ the k-scale normalization,[9,10] which imposes the following relation on the wave function:

$$\int_{-\infty}^{\infty}\phi_k^*(z)\phi_{k'}(z)dz=\delta(k-k') . \tag{3.7}$$

The details of the normalization procedure are shown in Appendix A. Then the normalized wave functions with gerade and ungerade parities are obtained as

$$\phi_k^g(z)=\left[\frac{e^{\pi\alpha}}{2\pi}\right]^{1/2}\frac{D_0^{(2)}W^{(1)}(x)-D_0^{(1)}W^{(2)}(x)}{(|D_0^{(1)}|^2+|D_0^{(2)}|^2)^{1/2}} , \tag{3.8a}$$

$$\phi_k^u(z)=\mathrm{sgn}(z)\left[\frac{e^{\pi\alpha}}{2\pi}\right]^{1/2}\frac{W_0^{(2)}W^{(1)}(x)-W_0^{(1)}W^{(2)}(x)}{(|W_0^{(1)}|^2+|W_0^{(2)}|^2)^{1/2}} , \tag{3.8b}$$

where the following notations are used:

$$W_0^{(j)} \equiv W^{(j)}(x=2ikz_0) , \tag{3.9a}$$

$$D_0^{(j)} \equiv \left.\frac{dW^{(j)}(x)}{dx}\right|_{x=2ikz_0} , \tag{3.9b}$$

for $j=1$ and 2. Figures 1(a) and 1(b) illustrate the probabilities $|\phi_k^g(z)|^2$ and $|\phi_k^u(z)|^2$ at the energy $E=\frac{1}{2}R^*$, where $R^*=\mu e^4/2\hbar^2\epsilon_1^2$ is the bulk effective Rydberg, for several values of the cutoff z_0/a_B^*. Unlike wave functions of bound states, oscillating components appear in the unbound wave functions. Now we are at the position to discuss the absorption spectra. We shall discuss separately two types of interband transitions, i.e., direct allowed and direct forbidden transitions.

a. Direct allowed transition. The optical-absorption coefficient for the direct allowed transition is given as[11,12]

$$K_a(\omega) \equiv \frac{1}{c\eta'}\frac{4\pi^2e^2}{m_0\omega}|\langle f|e^{i\eta' kr}\boldsymbol{\epsilon}\cdot\mathbf{P}|i\rangle|^2\rho(\hbar\omega) , \tag{3.10}$$

where i (f) denotes the ground state of the system (continuum exciton state), $\rho(\hbar\omega)$ is the joint density of states, η' the real part of the refractive index, $\boldsymbol{\epsilon}$ the polarization vector of light, P the total momentum of electrons, m_0 the free-electron mass, and ω is the frequency of the incident light. Here we note that the polarization characteristics are isotropic in our model because no mixing among valence subbands is taken into account. For the allowed transition in which $\langle c|\boldsymbol{\epsilon}\cdot\mathbf{p}|v\rangle \neq 0$, we can derive that

$$|\langle f|e^{i\eta' kr}\boldsymbol{\epsilon}\cdot\mathbf{P}|i\rangle|^2=m_0^2\omega^2|\phi_k^g(0)|^2|\langle c|\boldsymbol{\epsilon}\cdot\mathbf{r}|v\rangle|^2 ,$$

for a *gerade* wave function where c (v) denotes the conduction- (valence-) band Bloch function. Thus the intensity of the allowed transition is proportional to the probability for finding an electron and a hole at the same

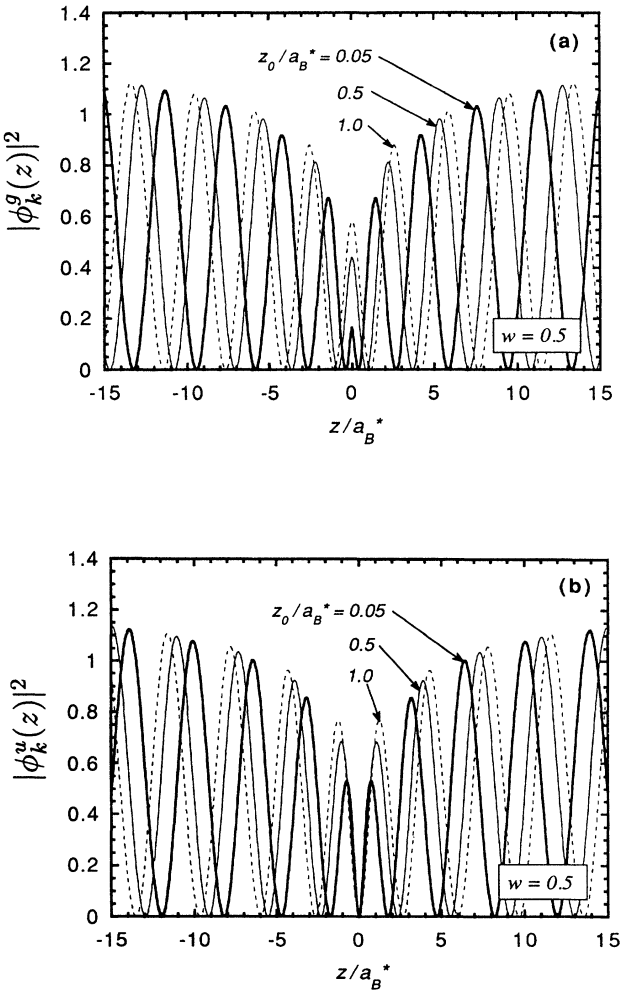

FIG. 1. (a) Squared moduli of unbound wave functions with a gerade parity $|\phi_k^g(z)|^2$ at $E=\frac{1}{2}R^*$ for $z_0/a_B^*=0.05$ (thick solid curve), 0.5 (thin solid curve), and 1.0 (dashed curve). (b) Squared moduli of unbound wave functions with an ungerade parity $|\phi_k^u(z)|^2$ at $E=\frac{1}{2}R^*$. The cutoff values are the same as in (a).

position. A characteristic feature of the 1D system is the van Hove singularity of the density of states ρ_{1D} at the band edge, i.e.,

$$\rho_{1D}(\hbar\omega)=\frac{2\mu}{\pi\hbar^2 k}\Theta(\hbar\omega-E_g)$$
$$=\frac{\sqrt{2\mu}}{\pi\hbar}\frac{1}{\sqrt{\hbar\omega-E_g}}\Theta(\hbar\omega-E_g)\ , \qquad (3.11)$$

where $\Theta(x)$ is the Heaviside step function and the band-gap energy[13] of the wire is defined as $E_g\equiv E_g^{\rm bulk}+\varepsilon_e^0+\varepsilon_h^0+\hbar^2K^2/2(m_e+m_h)$ [see also Eq. (2.7a)]. This is reflected in the spectrum associated with free electron-hole pair creation, which will be called the "free absorption" spectrum, i.e.,

$$K_a^{\rm 1D,free}(\omega)=8C_a\frac{w+\bar{E}_g}{\sqrt{w}}\ , \qquad (3.12)$$

where the photon energy and band-gap energy are scaled by $w=(\hbar\omega-E_g)/R^*$ and $\bar{E}_g\equiv E_g/R^*$, respectively, and

$$C_a=\frac{m_0R^*}{c\eta'\hbar}|\langle c|\boldsymbol{\varepsilon}\cdot\mathbf{r}|v\rangle|^2\ . \qquad (3.13)$$

In this energy scale, $\alpha=1/\sqrt{w}$ and $kz_0=(z_0/a_B^*)\sqrt{w}$. Taking account of the attractive interaction [Eq. (2.8a)] between an electron and a hole, the absorption intensity above the band edge is modified to

$$K_a^{\rm long}(\omega)=C_a e^{\pi\alpha}\frac{w+\bar{E}_g}{\sqrt{w}}\frac{|D_0^{(2)}W_0^{(1)}-D_0^{(1)}W_0^{(2)}|^2}{|D_0^{(1)}|^2+|D_0^{(2)}|^2}\ . \qquad (3.14)$$

Figure 2(a) shows optical-absorption spectra above E_g for various values of the cutoff z_0/a_B^*. Absorption intensities due to bound states below E_g are omitted in this figure. We find from Fig. 2(a) that the absorption strength is *smaller* than the free absorption $K_a^{\rm 1D,free}$ for any value of z_0 and that the band-edge singularity is removed. That is, the singular nature of the 1D joint density of states is not reflected in the interband absorption spectrum for an allowed transition when excitonic effects are taken into account. Additionally, the downward convexity of the spectra changes to the upward one as z_0 is decreased. More remarkably, the smaller the cutoff z_0 is, the weaker the absorption intensity becomes. As the cutoff length decreases ultimately to zero ($z_0\to 0$), where the attractive potential approaches the bare Coulomb potential, the interband absorption vanishes and the material becomes transparent even for the photon energy above the band gap.

These anomalous features can be seen more clearly in terms of the Sommerfeld factor. This factor, which is the ratio of the absorption coefficient of the unbound exciton to the free absorption, is given as

$$S_a^{\rm long}(\omega)\equiv\frac{K_a^{\rm long}(\omega)}{K_a^{\rm 1D,free}(\omega)}=\frac{e^{\pi\alpha}}{8}\frac{|D_0^{(2)}W_0^{(1)}-D_0^{(1)}W_0^{(2)}|^2}{|D_0^{(1)}|^2+|D_0^{(2)}|^2}\ , \qquad (3.15)$$

which is plotted in Fig. 2(b). The most striking features are $S_a^{\rm long}(\omega)<1$ for all $\hbar\omega>E_g$ and $S_a^{\rm long}(\hbar\omega=E_g)=0$ at the band edge. Comparison with 2D and 3D cases will be made later.

In this long-range case, the absorption spectrum in the $w>0$ region (true continuum above the band edge) connects smoothly with that in the $w<0$ region (quasicontinuum just below the band edge) where the absorption spectrum consists of many discrete lines due to the exciton

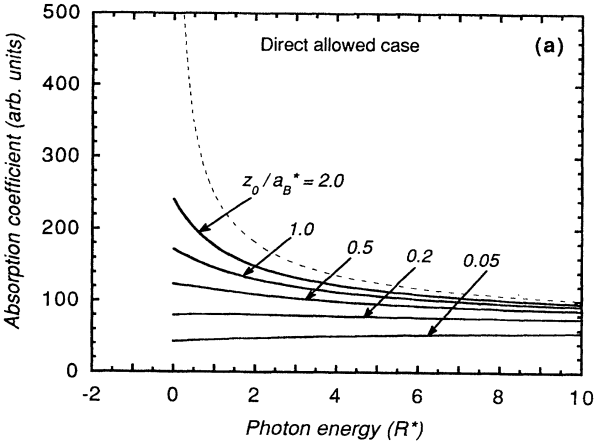

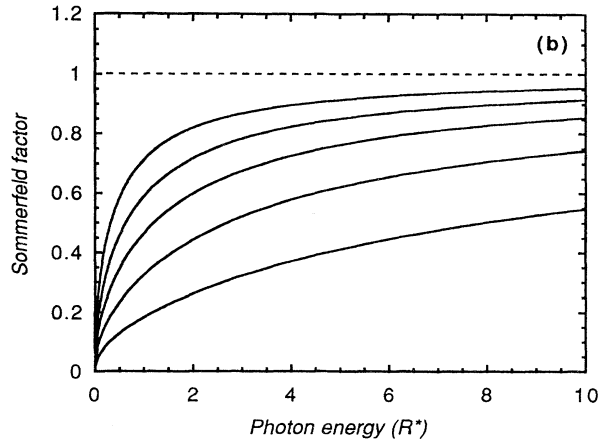

FIG. 2. (a) Absorption spectra due to a direct allowed transition in the case of long-range interaction are plotted by solid curves as a function of the scaled photon energy $w=(\hbar\omega-E_g)/R^*$ for several values of the cutoff length, i.e., $z_0/a_B^*=2.0$, 1.0, 0.5, 0.2, and 0.05 (from top to bottom). The dashed curve indicates the free absorption spectrum showing the band-edge divergence of the 1D system. Discrete exciton absorption lines below E_g ($w<0$) are not shown here. (b) Sommerfeld factors for the allowed transition for the same values of cutoff as in (a). These factors are always less than unity, indicating the suppressed interband absorption.

bound states. This is a characteristic feature of the *long-range* Coulomb interaction.

b. Direct forbidden transition. In the case of forbidden transition, on the other hand, $\langle c|\boldsymbol{\varepsilon}\cdot\mathbf{p}|v\rangle=0$. Here we can derive

$$|\langle f|e^{i\eta' kr}\boldsymbol{\varepsilon}\cdot\mathbf{P}|i\rangle|^2=\frac{\hbar}{2m_0^2}\left|\frac{d\phi_k^u(0)}{dz}\right|^2|\langle c|M|v\rangle|^2 ,$$

for an *ungerade* wave function, where an explicit form of $\langle c|M|v\rangle$ is given[12] as

$$\langle c|M|v\rangle=\sum_n\left[\frac{\langle c|p|n\rangle\langle n|\boldsymbol{\varepsilon}\cdot\mathbf{p}|v\rangle}{E_c-E_n}+\frac{\langle c|\boldsymbol{\varepsilon}\cdot\mathbf{p}|n\rangle\langle n|p|v\rangle}{E_v-E_n}\right], \tag{3.16}$$

where $|n\rangle$ is an intermediate state available in the $\mathbf{k}\cdot\mathbf{p}$ perturbation. Then the absorption coefficient is calculated as

$$K_f^{\text{long}}(\omega)=C_f e^{\pi\alpha}\frac{\sqrt{w}}{w+\bar{E}_g}\frac{|W_0^{(2)}D_0^{(1)}-W_0^{(1)}D_0^{(2)}|^2}{|W_0^{(1)}|^2+|W_0^{(2)}|^2} , \tag{3.17}$$

where

$$C_f=\frac{1}{c\eta'}\frac{4\hbar\sqrt{\mu}}{m_0^3 a_B^{*}\sqrt{2R^{*}}}|\langle c|M|v\rangle|^2 . \tag{3.18}$$

The results are illustrated in Fig. 3(a) for several values of cutoff z_0/a_B^{*}. Unlike in the direct allowed case, the absorption becomes stronger than the free absorption $K_f^{\text{1D,free}}$ for any value of z_0. Therefore, the Sommerfeld factor defined by

$$S_f^{\text{long}}(\omega)\equiv\frac{K_f^{\text{long}}(\omega)}{K_f^{\text{1D,free}}(\omega)}=\frac{e^{\pi\alpha}}{2}\frac{|W_0^{(2)}D_0^{(1)}-W_0^{(1)}D_0^{(2)}|^2}{|W_0^{(1)}|^2+|W_0^{(2)}|^2} \tag{3.19}$$

is larger than unity as shown in Fig. 3(b). As the cutoff z_0 is reduced, the absorption intensity for the forbidden transition becomes large in contrast with the case of allowed transition. This results from the fact that the derivative of the envelope function at the origin becomes large as the electron-hole attractive potential approaches the bare Coulomb potential. At the band edge, the Sommerfeld factor diverges because $K_f^{\text{1D,free}}(\hbar\omega=E_g)=0$.

2. *Coulomb potential with a cusp-type cutoff* $V_{\text{long}}^{A}(z)$

In this case the procedure for obtaining the unbound wave functions is almost the same as in the $V_{\text{long}}(z)$ case. Equation (3.1) is slightly changed to

$$\frac{d^2\phi(x)}{dx^2}-\left[\frac{1}{4}+\frac{i\alpha}{x}+\frac{m^2-\frac{1}{4}}{x^2}\right]\phi=0 , \tag{3.20}$$

where

$$m\equiv\left[\frac{1}{4}+2A\frac{z_0}{a_B^{*}}\right]^{1/2}\neq\frac{1}{2} . \tag{3.21}$$

The solutions of this equation have simpler forms than Eqs. (3.3), resulting in easier mathematical manipulations. The Sommerfeld factors for allowed and forbidden transitions are given, respectively, as

$$S_a^{\text{long},A}(\omega)=\frac{e^{\pi\alpha}}{2}[|W'_{-i\alpha,m}(2ikz_0)|^2+|V'_{-i\alpha,m}(2ikz_0)|^2]^{-1} , \tag{3.22a}$$

$$S_f^{\text{long},A}(\omega)=2e^{\pi\alpha}[|W_{-i\alpha,m}(2ikz_0)|^2+|V_{-i\alpha,m}(2ikz_0)|^2]^{-1} , \tag{3.22b}$$

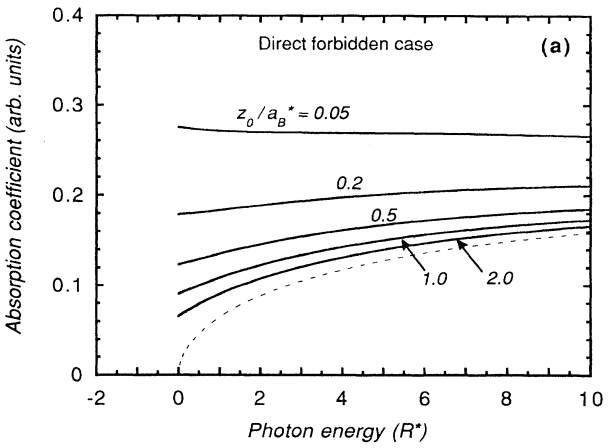

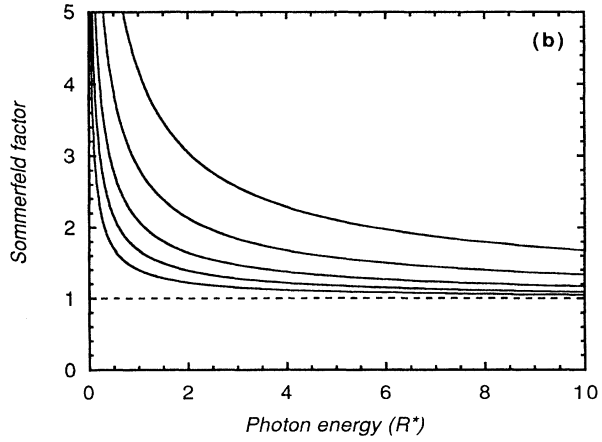

FIG. 3. (a) Absorption spectra due to a direct forbidden transition in the case of long-range interaction are plotted by solid curves as a function of the scaled photon energy w for several values of the cutoff, i.e., $z_0/a_B^{*}=2.0$, 1.0, 0.5, 0.2, and 0.05 (from bottom to top). The dashed curve indicates the free absorption spectrum. (b) Sommerfeld factors for the forbidden transition for the same values of cutoff as in (a).

where $W_{-i\alpha,m}(x)$ and $V_{-i\alpha,m}(x)$ are the basis solutions of Eq. (3.20), which are expressed as

$$W_{-i\alpha,m}(x)\equiv\frac{\Gamma(-2m)}{\Gamma(\frac{1}{2}-m+i\alpha)}M_{-i\alpha,m}(x)+\frac{\Gamma(2m)}{\Gamma(\frac{1}{2}+m+i\alpha)}M_{-i\alpha,-m}(x)\ , \tag{3.23a}$$

$$V_{-i\alpha,m}(x)\equiv-i\frac{e^{-im\pi}\Gamma(-2m)}{\Gamma(\frac{1}{2}-m-i\alpha)}M_{-i\alpha,m}(x)-i\frac{e^{im\pi}\Gamma(2m)}{\Gamma(\frac{1}{2}+m-i\alpha)}M_{-i\alpha,-m}(x)\ , \tag{3.23b}$$

$$W'_{-i\alpha,m}(x)\equiv\frac{d}{dx}W_{-i\alpha,m}(x)\ , \tag{3.23c}$$

$$V'_{-i\alpha,m}(x)\equiv\frac{d}{dx}V_{-i\alpha,m}(x)\ , \tag{3.23d}$$

with the use of a confluent hypergeometric function

$$M_{-i\alpha,\pm m}(x)\equiv e^{-x/2}x^{\pm m+1/2}F(\tfrac{1}{2}\pm m+i\alpha,1\pm2m;x)\ . \tag{3.24}$$

In deriving the Sommerfeld factors, the Wronskian relation is used:

$$W_{-i\alpha,m}(x)V'_{-i\alpha,m}(x)-V_{-i\alpha,m}(x)W'_{-i\alpha,m}(x)=e^{\pi\alpha}\ . \tag{3.25}$$

Although expressions of the Sommerfeld factors for the potential $V^{A}_{\rm long}(z)$ [Eqs. (3.22)] have quite different forms from those in the case of $V_{\rm long}(z)$ [Eqs. (3.15) and (3.19)], the numerical results are almost the same for a small value of A. In fact, the two results coincide with each other in the $A\to0$ limit. Precisely speaking, the Sommerfeld factor for an allowed (forbidden) transition is slightly larger (smaller) than Eq. (3.15) [Eq. (3.19)] in the case of $A>0$ because the electron-hole attractive potential is weaker for $A>0$ than for $A=0$.

B. Short-range interaction case

In solving the 1D Schrödinger equation with the short-range potential $V_{\rm short}(z)$ [Eq. (2.8c)], we employ a new independent variable $\xi\equiv\tanh(z/\zeta)$ and define a wave number by $k=\sqrt{2\mu E}/\hbar$. When the wave function $\phi_k(z)$ is substituted by $\tilde{\phi}_k(\xi)$ as $\phi_k=(1-\xi^2)^{-ik\zeta/2}\tilde{\phi}_k(\xi)$, the wave equation becomes a hypergeometric equation, i.e.,

$$u(1-u)\frac{d^2\tilde{\phi}_k}{du^2}+(1-ik\zeta)(1-2u)\frac{d\tilde{\phi}_k}{du}+(ik\zeta+s)(-ik\zeta+s+1)\tilde{\phi}_k=0\ , \tag{3.26}$$

where $u\equiv(1-\xi)/2$. In the following the depth and width of the potential are scaled by the effective Rydberg and bulk Bohr radius as $\bar{V}_0\equiv V_0/R^*$ and $\bar{\zeta}\equiv\zeta/a_B^*$, respectively, and we measure the photon energy and band gap as $w\equiv(\hbar\omega-E_g)/R^*$ and $\bar{E}_g\equiv E_g/R^*$, respectively, as employed in the long-range case. In this scaling we have $k\zeta=\bar{\zeta}\sqrt{w}$. Here s is an important parameter to characterize the short-range interaction, which is defined as

$$s\equiv\tfrac{1}{2}[-1+(1+4\bar{V}_0\bar{\zeta}^2)^{1/2}]>0\ . \tag{3.27}$$

Then the envelope function $\phi_k(z)$ for unbound states can be written in a linear combination of two basis solutions given as

$$f_k(\xi)\equiv(1-\xi^2)^{-ik\zeta/2}\times F\left[-ik\zeta-s,-ik\zeta+s+1,1-ik\zeta;\frac{1-\xi}{2}\right]\ , \tag{3.28a}$$

$$g_k(\xi)\equiv(1-\xi^2)^{-ik\zeta/2}\left[\frac{1-\xi}{2}\right]^{ik\zeta}\times F\left[-s,s+1,1+ik\zeta;\frac{1-\xi}{2}\right]\ . \tag{3.28b}$$

Similarly to Sec. III A, there are two types of parity (gerade and ungerade) of the unbound wave functions. As shown in Appendix A, the normalized wave functions are given as

$$\phi^g_k(z)=\frac{1}{\sqrt{2\pi}}\frac{g'_k(0)f_k(\xi)-f'_k(0)g_k(\xi)}{[|f'_k(0)|^2+|g'_k(0)|^2]^{1/2}}\ , \tag{3.29a}$$

$$\phi^u_k(z)=\frac{1}{\sqrt{2\pi}}\frac{g_k(0)f_k(\xi)-f_k(0)g_k(\xi)}{[|f_k(0)|^2+|g_k(0)|^2]^{1/2}}\ , \tag{3.29b}$$

where a prime stands for the derivative with respect to ξ. Here we note that there is another set of solutions of Eq. (3.26) around $u=1$ ($z\to-\infty$) in addition to Eqs. (3.28) around $u=0$ ($z\to\infty$). These are symmetric and antisymmetric with respect to $u=\frac{1}{2}$ ($z=0$) for gerade and ungerade parities, respectively, and coincide with Eqs. (3.28) at $z=0$ because of the symmetry of the potential. Therefore, it is sufficient to consider only Eqs. (3.28) in our discussion of absorption spectra.

a. Direct allowed transition. Taking account of the short-range interaction between an electron and a hole, the absorption intensity above the band edge is given as

$$K_a^{\rm short}(\omega)=4C_a\frac{w+\bar{E}_g}{\sqrt{w}}\frac{|g'_k(0)f_k(0)-f'_k(0)g_k(0)|^2}{|f'_k(0)|^2+|g'_k(0)|^2}\ , \tag{3.30}$$

where C_a is given in Eq. (3.13). Then the Sommerfeld factor is calculated as

$$S_a^{\rm short}(\omega)=\frac{1}{2}\frac{|g'_k(0)f_k(0)-f'_k(0)g_k(0)|^2}{|f'_k(0)|^2+|g'_k(0)|^2}\ . \tag{3.31}$$

Figure 4(a) shows optical-absorption spectra above E_g for various values of the potential depth $\bar{V}_0$ with a fixed value of the potential width $\bar{\zeta}=2.0$. Similarly, Fig. 5(a) shows the absorption spectra for several values of $\bar{\zeta}$ with a fixed value of the potential depth $\bar{V}_0=2.0$. From these

figures we find that the absorption strength is smaller than the free absorption $K_a^{1D,free}$ for any values of $\bar{V}_0$ and $\bar{\zeta}$ in the same way as in the long-range case. The deeper the potential is ($\bar{V}_0 \to \infty$), the weaker the absorption intensity becomes. Thus the global characteristics of the spectra are the same as in the long-range case. The Sommerfeld factor also shows a similar behavior, i.e., $S_a^{short}(\omega) < 1$ for all $\hbar\omega > E_g$, as shown in Figs. 4(b) and 5(b).

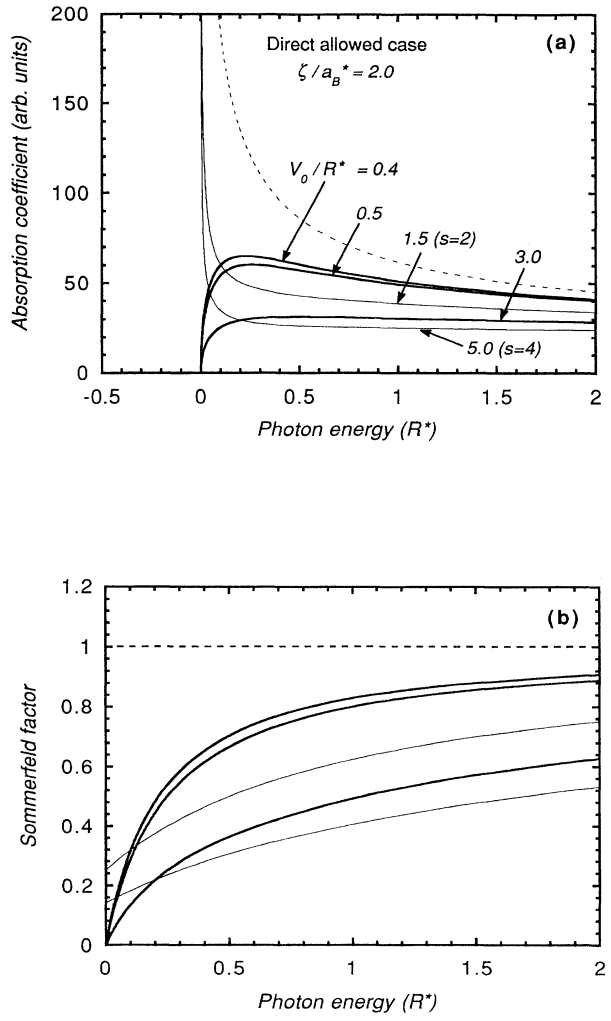

FIG. 4. (a) Absorption spectra due to a direct allowed transition in the case of short-range interaction are plotted by solid curves as a function of the scaled photon energy $w = (\hbar\omega - E_g)/R^*$ for several values of the potential depth, i.e., $\bar{V}_0 = 0.4$, 0.5, 1.5, 3.0, and 5.0 (from top to bottom) with a fixed potential width $\bar{\zeta} = 2.0$. These correspond to $s = 0.86$, 1.0, 2.0, 3.0, and 4.0, respectively. When s is an even integer, the absorption intensity diverges at the edge as shown by thin solid curves for $s = 2$ and 4. The thin-dashed curve indicates the free absorption spectrum. Absorption lines due to discrete exciton states below E_g ($w < 0$) are not shown here. (b) Sommerfeld factors for the allowed transition for the same values of parameters as in (a).

A major difference from the long-range case appears in the behavior at the band edge ($w \simeq 0$). When the parameter s is an even integer, $s = 2,4,6, \ldots$, the absorption intensity near the band edge diverges to infinity, while it becomes zero for other cases; that is,

$$K_a^{short}(\hbar\omega = E_g) = \begin{cases} \infty, & s = 2,4,6, \ldots \\ 0, & \text{otherwise} . \end{cases} \tag{3.32}$$

The mathematical origin of this divergence is shown in Appendix B. In the case of short-range potential, the number of the bound states becomes *finite* in contrast to the long-range case. As will be discussed in the next sec-

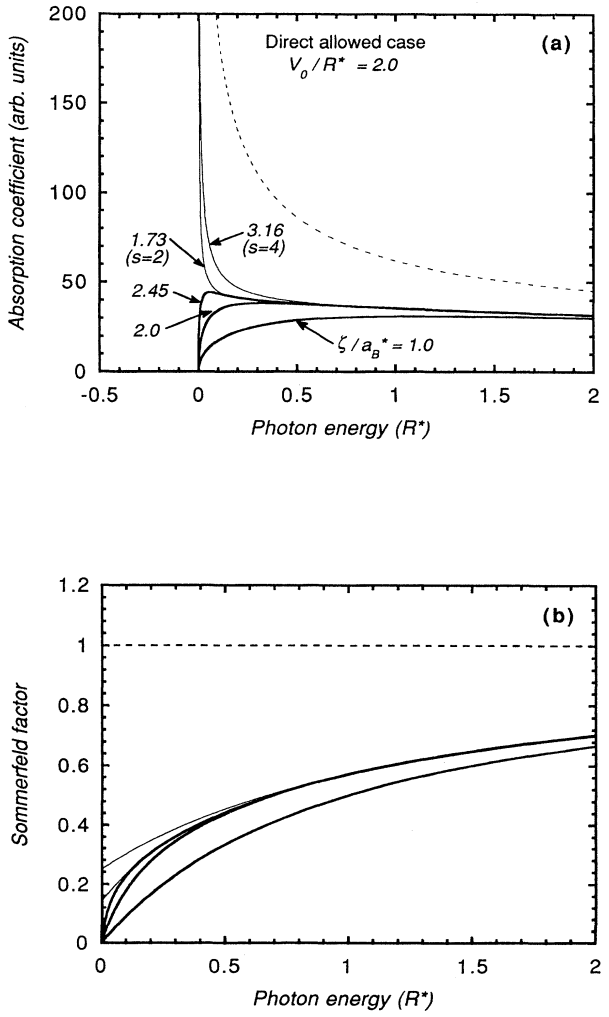

FIG. 5. (a) Absorption spectra due to a direct allowed transition in the case of short-range interaction are plotted by solid curves for several values of the potential width, i.e., $\bar{\zeta} = \sqrt{10}$, $\sqrt{3}$, $\sqrt{6}$, 2.0, and 1.0 (from top to bottom) with a fixed potential depth $\bar{V}_0 = 2.0$. These correspond to $s = 4.0$, 2.0, 3.0, 2.37, and 1.0, respectively. When s is an even integer, the absorption intensity diverges at the edge as shown by thin solid curves for $s = 2$ and 4. (b) Sommerfeld factors for the allowed transition for the same values of parameters as in (a).

tion, the number is given as $N=[s]$, where [ ] is Gauss' symbol. Therefore, there is no quasicontinuum region in the absorption spectra just below the band edge. That is, there exists an "energy gap" between the band edge (the bottom of the conduction band) and the highest-energy bound state unless s is an integer. Thus the absorption line is *discontinuous* near the band edge, resulting in the zero absorption at the edge. When $s=2,4,6,\ldots$, however, the corresponding highest bound state ($n=2,4,6,\ldots$), which is direct allowed, is degenerate to the band edge. Then the absorption spectra show a divergence there. Correspondingly, $S_a^{\rm short}(\hbar\omega=E_g)$ at the band edge is not always zero, i.e.,

$$S_a^{\rm short}(\hbar\omega=E_g)\begin{cases}>0, & s=2,4,6,\ldots\\ =0, & \text{otherwise}.\end{cases} \tag{3.33}$$

The analytical expressions of $S_a^{\rm short}(\hbar\omega=E_g)$ for $s=2,4,6,\ldots$ are so complicated that they are not shown here. The numerical values of $S_a^{\rm short}(\hbar\omega=E_g)$ for $s=2$ and 4 are 0.250 and 0.141, respectively.

b. Direct forbidden transition. In the case of forbidden transition, on the other hand, the absorption coefficient and corresponding Sommerfeld factor are evaluated as

$$K_f^{\rm short}(\omega)=\frac{C_f}{\bar{\xi}^2\sqrt{w}\,(w+\bar{E}_g)}\times\frac{|g_k(0)f_k'(0)-f_k(0)g_k'(0)|^2}{|f_k(0)|^2+|g_k(0)|^2}, \tag{3.34}$$

$$S_f^{\rm short}(\omega)=\frac{1}{2\bar{\xi}^2 w}\frac{|g_k(0)f_k'(0)-f_k(0)g_k'(0)|^2}{|f_k(0)|^2+|g_k(0)|^2}, \tag{3.35}$$

where C_f is given in Eq. (3.18). The results are illustrated in Figs. 6 and 7 for several values of the width $\bar{\xi}$ and depth $\bar{V}_0$ of the electron-hole attractive potential. The absorption intensity becomes stronger than the free absorption $K_f^{\rm 1D,free}$. As the depth $\bar{V}_0$ becomes large, the absorption due to the forbidden transition becomes strong. The Sommerfeld factor is always larger than unity, i.e., $S_f^{\rm short}(\omega)>1$ for all $\hbar\omega>E_g$. Thus global features are similar to those in the long-range case. However, there is a difference in the behaviors near the edge. When the parameter s is an odd integer, $s=1,3,5,\ldots$, the corresponding highest bound state ($n=1,3,5,\ldots$), which is direct forbidden, is degenerate to the band edge. As a result, the absorption intensity near the band edge diverges to infinity for $s=1,3,5,\ldots$, while it becomes zero for other cases; that is,

$$K_f^{\rm short}(\hbar\omega=E_g)=\begin{cases}\infty, & s=1,3,5,\ldots\\ 0, & \text{otherwise}.\end{cases} \tag{3.36}$$

Correspondingly, the Sommerfeld factor at the band edge becomes

$$S_f^{\rm short}(\hbar\omega=E_g)\begin{cases}=\infty, & s=1,3,5,\ldots\\ <\infty, & \text{otherwise}.\end{cases} \tag{3.37}$$

In Figs. 6 and 7, the numerical values of $S_f^{\rm short}(\hbar\omega=E_g)$ for $s=0.86$, 2.0, 2.37, and 4.0 are 47.5, 4.00, 6.58, and 7.11, respectively.

In summary, global characteristics of the interband absorption spectra are the same as in the long-range case; namely, the Sommerfeld factor for allowed (forbidden) transition is smaller (larger) than unity for any photon energy $\hbar\omega>E_g$. Thus these features can be considered as universal in the 1D system.

IV. BOUND STATES AND THEIR OSCILLATOR STRENGTH

In the preceding section, we clarified the interband absorption above the band edge associated with creation of

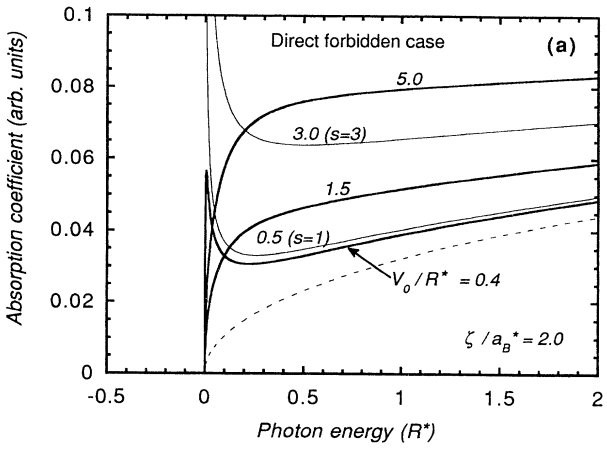

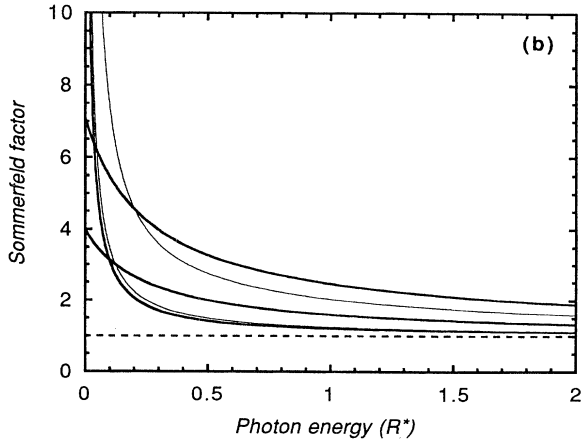

FIG. 6. (a) Absorption spectra due to a direct forbidden transition in the case of short-range interaction are plotted by solid curves for several values of the potential depth, i.e., $\bar{V}_0=0.4$, 0.5, 1.5, 3.0, and 5.0 (from bottom to top) with a fixed potential width $\bar{\xi}=2.0$. These correspond to $s=0.86$, 1.0, 2.0, 3.0, and 4.0, respectively. When s is an odd integer, the absorption intensity diverges at the edge as shown by thin solid curves for $s=1$ and 3. (b) Sommerfeld factors for the forbidden transition for the same values of parameters as in (a).

the *unbound* excitons. In this section the optical absorption due to the exciton *bound states* will be examined. The main purpose is twofold: (i) to clarify the oscillator strength of the bound states in relation to the interband absorption discussed in Sec. III and (ii) to understand comprehensively optical properties of the 1D excitonic bound state for both cases of the long- and short-range attractive potentials.

A. Long-range interaction case

It is convenient for the study of bound states to use an energy scaling and a new independent variable, i.e., $E \equiv -R^*/\nu^2$ and $x \equiv 2(|z|+z_0)/(\nu a_B^*)$. Here x is real and ν ($\nu>0$) is a real parameter to be determined. The 1D Schrödinger equation then becomes a Whittaker equation, which is given by Eq. (3.1), with a substitution of $i\alpha$ by $-\nu$. A solution bounded for $|z|\to\infty$ is given as

$$\phi_\nu(z)=N_\nu W^{(2)}_{\nu,1/2}(x) \equiv N_\nu x e^{-x/2}\Gamma(1+\nu)[F(1-\nu,2;x)-G(1-\nu,2;x)] , \tag{4.1}$$

where N_ν is a normalization constant and $F(\alpha,\gamma;z)$ and $G(\alpha,\gamma;z)$ have been defined in Eqs. (3.5). In fact, Eq. (4.1) has an asymptotic form of $-N_\nu e^{-\nu\pi}|x|^\nu e^{-|x|/2}$, which approaches zero for $|x|\to\infty$.

Because of the symmetry of the potential with respect to the origin ($z=0$), the parity of a wave function for a bound state should be either odd or even. The odd and even parities impose the following relations on the wave function, respectively:

$$W^{(2)}_{\nu,1/2}\left[x=\frac{2z_0}{\nu a_B^*}\right]=0 \quad \text{for odd} , \tag{4.2a}$$

$$\frac{d}{dx}W^{(2)}_{\nu,1/2}(x)\bigg|_{x=2z_0/\nu a_B^*}=0 \quad \text{for even} . \tag{4.2b}$$

From these relations the parameter ν and energy of bound states are determined. Although Eqs. (4.2) cannot be solved analytically, they are approximately solved by Loudon[4] in the small cutoff case ($z_0/a_B^* \ll 1$) as

$$\nu=\nu_n=\begin{cases} \nu_n^{\text{odd}} \simeq n+\dfrac{2z_0}{a_B^*} & \text{for odd states} , \\ \nu_n^{\text{even}} \simeq n-\dfrac{1}{\ln(2z_0/na_B^*)} & \text{for even states} , \end{cases} \tag{4.3}$$

respectively, for $n=1,2,3,\ldots$. These correspond to the excited bound states of exciton. Substituting these ν_n into $E_n \equiv -R^*/\nu_n^2$, the eigenenergy of the bound states is obtained. The lowest bound state has special characteristics. For this state, ν_0 satisfies

$$\ln\left[\frac{2z_0}{\nu_0 a_B^*}\right]+\frac{1}{2\nu_0}=0 . \tag{4.4}$$

As the cutoff decreases ($z_0\to 0$), ν_0 approaches zero, resulting in a very large binding energy.

In the limit of $z_0\to 0$, the odd- and even-parity wave functions for the bound states except the lowest state are characterized by $\nu_n^{\text{odd}}=\nu_n^{\text{even}}=n\equiv 1,2,3,\ldots$, and are given as

$$\phi_n^{\text{odd}}(z)=\left[\frac{2}{(a_B^*)^3 n^5 (n!)^2}\right]^{1/2} z\exp\left[-\frac{|z|}{na_B^*}\right]L_n^1\left[\frac{2|z|}{na_B^*}\right] , \tag{4.5a}$$

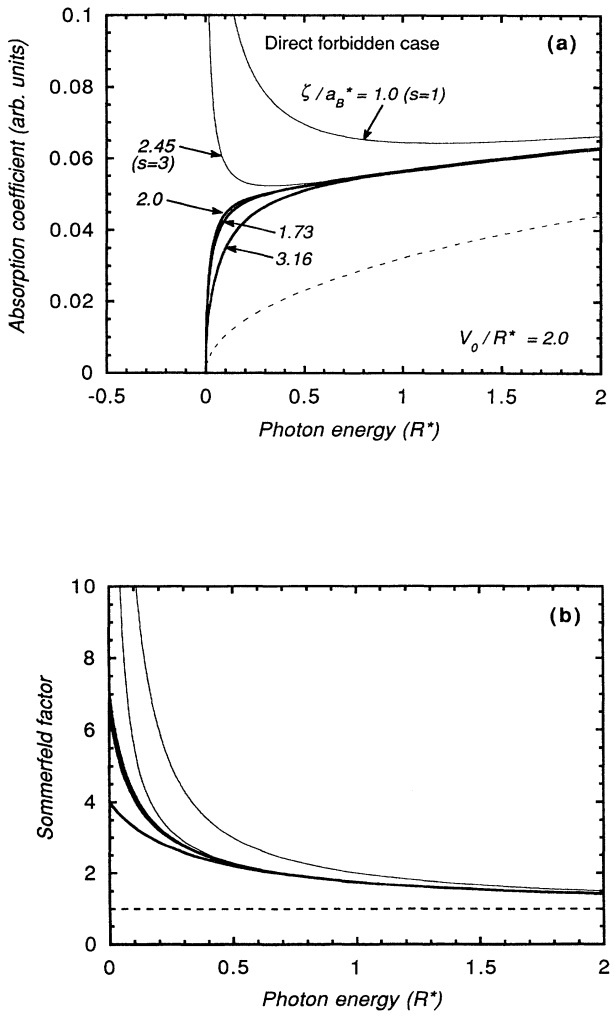

FIG. 7. (a) Absorption spectra due to a direct forbidden transition in the case of short-range interaction are plotted by solid curves for several values of the potential width, i.e., $\bar{\zeta}=\sqrt{10}$, $\sqrt{3}$, 2.0, $\sqrt{6}$, and 1.0 (from bottom to top) with a fixed potential depth $\bar{V}_0=2.0$. These correspond to $s=4.0$, 2.0, 2.37, 3.0, and 1.0, respectively. When s is an odd integer, the absorption intensity diverges at the edge as shown by thin solid curves for $s=1$ and 3. (b) Sommerfeld factors for the forbidden transition for the same values of parameters as in (a).

$$\phi_n^{\text{even}}(z)=\left[\frac{2}{(a_B^*)^3 n^5 (n!)^2}\right]^{1/2}|z|\exp\left[-\frac{|z|}{na_B^*}\right]L_n^1\left[\frac{2|z|}{na_B^*}\right], \tag{4.5b}$$

where $L_n^1(x)$ is the associated Laguerre polynomial. Here we note that not only the odd-parity wave function but also the *even*-parity one vanishes at the origin to cancel the singularity of the potential. The eigenenergies of these bound states are doubly degenerate, i.e.,

$$E_n^{\text{odd}}=E_n^{\text{even}}=-\frac{R^*}{n^2}\ , \quad n=1,2,3,\ldots, \tag{4.6}$$

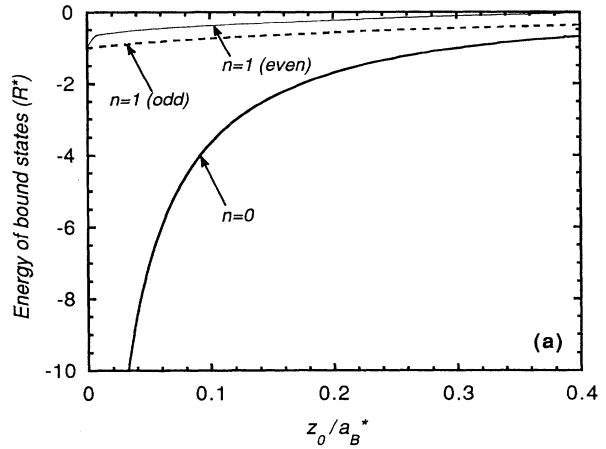

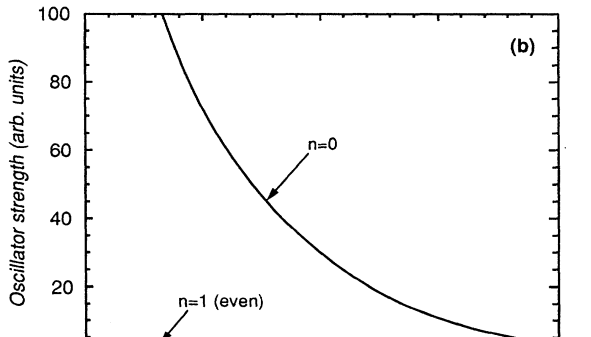

FIG. 8. (a) Eigenenergy of the lowest exciton state ($n=0$) in the case of long-range interaction is plotted by a thick solid curve as a function of the cutoff z_0/a_B^*. The odd- and even-parity states of the $n=1$ exciton are shown by dashed and thin solid curves, respectively. In the limit of $z_0\to 0$, the energy of the lowest state diverges and the energies of the pair of $n=1$ states are degenerate at $E=-R^*$. (b) The oscillator strength of the lowest exciton state and the $n=1$ even-parity exciton state is plotted by thick and thin solid curves, respectively, as a function of the cutoff. Strong concentration of the oscillator strength on the lowest exciton state is clearly seen. The oscillator strength of other even-parity exciton states is very small.

showing the Balmer energy series. This system violates the well-known "nondegeneracy theorem" for bound states in the 1D system, resulting from a singularity of the potential at the origin.[4] For the lowest bound state, on the other hand, the wave function and its eigenenergy are given as

$$\phi_0(z)=\lim_{\nu_0\to 0}\frac{\exp(-|z|/\nu_0 a_B^*)}{(\nu_0 a_B^*)^{1/2}}=\sqrt{\delta(z)}\ , \tag{4.7}$$

$$E_0=-\infty\ , \tag{4.8}$$

respectively.

In this case of long-range interaction, there exist infinitely many bound states below the band edge. Among them, only the lowest-energy state shows anomalous behavior as the cutoff decreases. Figure 8(a) shows the energy of the first three bound states (corresponding to $n=0$ and 1) as a function of the cutoff z_0. As $z_0\to 0$, the energy of the lowest state become negatively infinite, indicating the divergence of the binding energy. This is a peculiar feature of the 1D exciton. Other bound states become doubly degenerate for odd and even parities at finite energies $-R^*/n^2$ ($n=1,2,3,\ldots$).

The oscillator strength of the bound state with an even or odd parity, which is one-photon allowed or forbidden, respectively, is defined as

$$f_n^a\equiv\frac{2m_0\omega}{\hbar}|\langle c|\boldsymbol{\varepsilon}\cdot\mathbf{r}|v\rangle|^2|\phi_n^{\text{even}}(0)|^2\ , \tag{4.9a}$$

$$f_n^f\equiv\frac{1}{m_0^3\omega}|\langle c|M|v\rangle|^2\left|\frac{d\phi_n^{\text{odd}}(0)}{dz}\right|^2\ , \tag{4.9b}$$

for $n=1,2,3,\ldots$. We plot f_0^a and f_1^a in Fig. 8(b) as a function of the cutoff z_0 to illustrate the *anomalously strong concentration of the oscillator strength on the lowest-energy bound state.* The oscillator strength of other bound states with an even parity vanishes completely in the limit of $z_0\to 0$, resulting from their vanishing wave function at $z=0$ [see Eq. (4.5b)]. For the odd-parity states, there occurs no concentration of the oscillator strength on f_1^f. In fact, f_1^f is finite even when $z_0\to 0$, in distinct contrast to f_0^a, which shows a divergence.

In the case of the potential $V_{\text{long}}^A(z)$, the wave function for bound states is given by $\phi_\nu(z)=N_\nu W_{\nu,m}(x)$, where m and $W_{\nu,m}$ have been defined in Eqs. (3.21) and (3.23a), respectively. Properties of bound states are almost the same as in the $V_{\text{long}}(z)$ case. For details, refer to Ref. 5.

B. Short-range interaction case

The eigenenergy of a bound state ($E<0$) is measured by a dimensionless parameter, i.e., $\eta\equiv\xi\sqrt{-2\mu E}/\hbar$. After a substitution of $\phi=(1-\xi^2)^{\eta/2}\bar{\phi}(\xi)$, the wave equation for $\bar{\phi}(\xi)$ becomes a hypergeometric equation given by Eq. (3.26) with a substitution of $ik\xi$ by $-\eta$. A solution, which is finite as $z\to+\infty$ ($u\to 0+$), is given by a hypergeometric function, i.e., $\bar{\phi}(u)\propto F(\eta-s,\eta+s+1,\eta+1;u)$, where $u=(1-\xi)/2$. Here $\xi=\tanh(z/\zeta)$ and s has been defined in Eq. (3.27). The wave functions of the bound states are further required to be bounded

also as $z\to-\infty$ ($u\to1$). Therefore, $s-\eta$ should be a non-negative integer,[14] i.e., $\eta=s-n$ with $n\equiv0,1,2,3\ldots$. This integer n is an index of the bound states. As a result, the wave function $\phi_n(z)$ and eigenenergy E_n of the bound state are given as

$$\phi_n(z)=N_n\left[1-\tanh^2\left[\frac{z}{\zeta}\right]\right]^{(s-n)/2}\times F(-n,2s+1-n,s+1-n;u)\ , \tag{4.10}$$

$$E_n=-\frac{R^*}{4\bar{\zeta}^2}[(1+4\bar{V}_0\bar{\zeta}^2)^{1/2}-(2n+1)]^2=-\frac{R^*}{\bar{\zeta}^2}(s-n)^2\ , \tag{4.11}$$

where N_n is a normalization constant given by

$$N_n^{-2}=\frac{4^{s-n}\zeta}{2}\int_0^1[u(1-u)]^{s-n-1}\times[F(-n,2s+1-n,s+1-n;u)]^2du\ . \tag{4.12}$$

Because of a condition $s-n>0$, the index n is bounded as $n=0,1,2,\ldots,[s]$. Therefore, the nth bound state[15] can exist only when $s>n$. Then the number of bound states becomes *finite* in distinct contrast to the case of long-range interaction.

The oscillator strength of the bound state is calculated for one-photon allowed ($n=0,2,4,\ldots$) and forbidden ($n=1,3,5,\ldots$) cases as

$$f_n^a=\frac{2m_0R^*}{\hbar^2}|\langle c|\boldsymbol{\varepsilon}\cdot\mathbf{r}|v\rangle|^2(\bar{E}_g+w_n)N_n^2\times[F(-n,2s+1-n,s+1-n;\tfrac{1}{2})]^2\ , \tag{4.13a}$$

$$f_n^f=\frac{\hbar}{m_0^3R^*}|\langle c|M|v\rangle|^2(\bar{E}_g+w_n)^{-1}\left|\frac{d}{dz}\phi_n(0)\right|^2\ , \tag{4.13b}$$

respectively, where $w_n\equiv E_n/R^*=-(s-n)^2/\bar{\zeta}^2$. We shall list the wave functions, the eigenenergies, and their oscillator strength for the first three bound states. (i) The lowest-energy state ($n=0$) always exists for arbitrary values of s, whose wave function, eigenenergy, and oscillator strength are given as

$$\phi_0(z)=\frac{1}{2^{s-1}}\frac{1}{\sqrt{2\zeta B(s,s)}}\left[1-\tanh^2\left[\frac{z}{\zeta}\right]\right]^{s/2}\ , \tag{4.14a}$$

$$\frac{E_0}{R^*}=-\frac{s^2}{\bar{\zeta}^2}\ , \tag{4.14b}$$

$$f_0^a=\frac{2m_0R^*}{\hbar a_B^*}|\langle c|\boldsymbol{\varepsilon}\cdot\mathbf{r}|v\rangle|^2\left[\bar{E}_g-\frac{s^2}{\bar{\zeta}^2}\right]\frac{1}{2^{2s-1}\bar{\zeta}B(s,s)}\ , \tag{4.14c}$$

where $B(x,y)$ is the beta function. (ii) Only when $s>1$ (i.e., $\bar{V}_0\bar{\zeta}^2>2$), does the first excited state exist which is one-photon forbidden. The results are

$$\phi_1(z)=N_1\left[1-\tanh^2\left[\frac{z}{\zeta}\right]\right]^{(s-1)/2}\tanh\left[\frac{z}{\zeta}\right]\ , \tag{4.15a}$$

$$\frac{E_1}{R^*}=-\frac{(s-1)^2}{\bar{\zeta}^2}\ , \tag{4.15b}$$

$$f_1^f=\frac{\hbar}{m_0^3(a_B^*)^3R^*}|\langle c|M|v\rangle|^2\left[\bar{E}_g-\frac{(s-1)^2}{\bar{\zeta}^2}\right]^{-1}\frac{N_1^2}{\bar{\zeta}^2}\ , \tag{4.15c}$$

where N_1 is a normalization constant given by

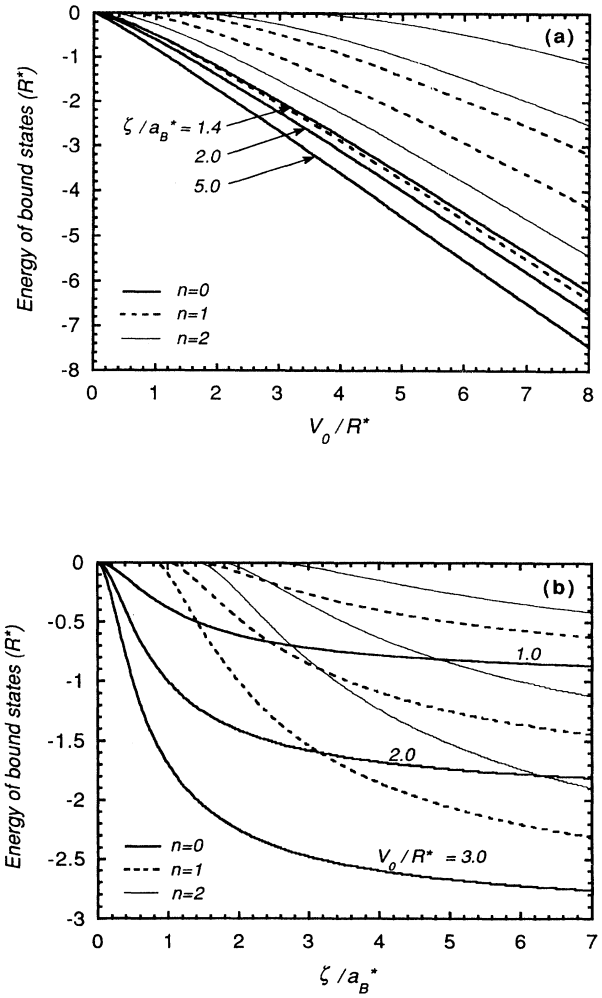

FIG. 9. (a) Eigenenergies of the exciton states in the case of short-range interaction are plotted by thick solid curves for the $n=0$ state (with an even parity), dashed curves for $n=1$ state (odd parity), and thin solid curves for $n=2$ state (even parity), respectively, as a function of the potential depth for fixed values of the potential width, $\bar{\zeta}=5.0$, 2.0, and 1.4 (from bottom to top). (b) The eigenenergies as a function of the potential width for fixed values of the potential depth, $\bar{V}_0=3.0$, 2.0, and 1.0 (from bottom to top). The meaning of the thick and thin solid curves and the dashed curves is the same as in (a).

$$N_1^{-2}=2^{2s-3}\bar{\zeta}[B(s-1,s-1)-4B(s,s-1)+4B(s+1,s-1)]\ . \tag{4.16}$$

(iii) The second bound state which is one-photon allowed appears when $s>2$ (i.e., $\bar{V}_0\bar{\zeta}^2>6$) as

$$\phi_2(z)=N_2\left[1-\tanh^2\left[\frac{z}{\zeta}\right]\right]^{s/2-1}\left[1-\frac{c}{4}+\frac{c}{4}\tanh^2\left[\frac{z}{\zeta}\right]\right]\ , \tag{4.17a}$$

$$\frac{E_2}{R^*}=-\frac{(s-2)^2}{\bar{\zeta}^2}\ , \tag{4.17b}$$

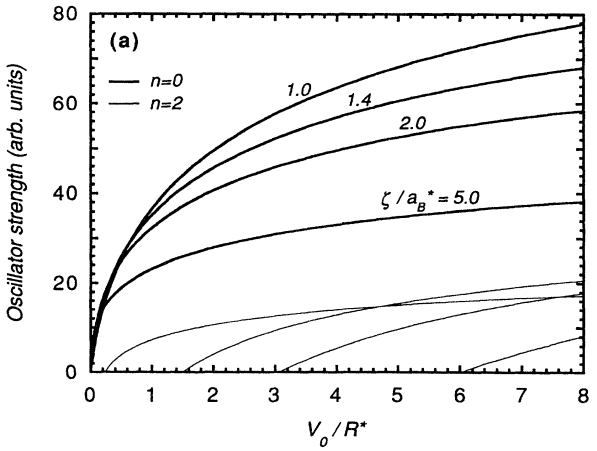

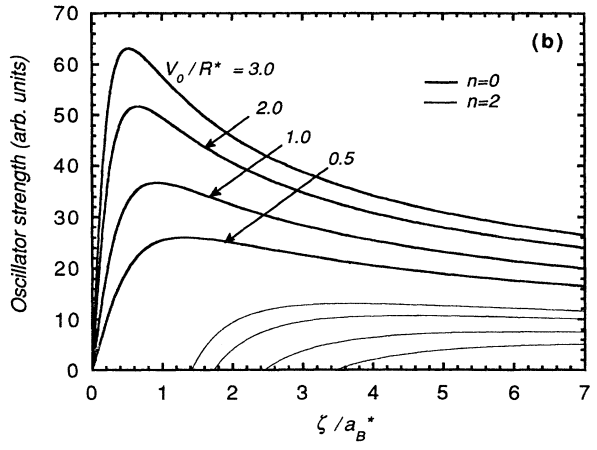

FIG. 10. (a) Oscillator strength of the even-parity exciton states in the case of short-range interaction is plotted by thick solid curves for the $n=0$ state and by thin solid curves for the $n=2$ state, respectively, as a function of the potential depth for several values of the potential width, $\bar{\zeta}=5.0$, 2.0, 1.4, and 1.0 (from bottom to top for thick curves, from left to right for thin curves). (b) The oscillator strength as a function of the potential width for several values of the potential depth, $\bar{V}_0=3.0$, 2.0, 1.0, and 0.5 (from top to bottom). The meaning of the thick and thin solid curves is the same as in (a).

$$f_2^a=\frac{2m_0R^*}{\hbar a_B^*}|\langle c|\boldsymbol{\varepsilon}\cdot\mathbf{r}|v\rangle|^2\left[\bar{E}_g-\frac{(s-2)^2}{\bar{\zeta}^2}\right]\frac{N_2^2}{4(s-1)^2}\ , \tag{4.17c}$$

where

$$c=\frac{2(2s-1)}{s-1}\ , \tag{4.18a}$$

$$N_2^{-2}=2^{2s-5}\bar{\zeta}[B(s-2,s-2)-2cB(s-1,s-2)+c(c+2)B(s,s-2)-2c^2B(s+1,s-2)+c^2B(s+2,s-2)]\ . \tag{4.18b}$$

The eigenenergies of the bound states are plotted in Figs. 9(a) and 9(b) as a function of the potential depth $\bar{V}_0$ and width $\bar{\zeta}$, respectively. The binding energy increases with increasing $\bar{V}_0$ for a fixed value of $\bar{\zeta}$. In the limit of $\bar{\zeta}\to\infty$, the binding energy approaches $\bar{V}_0$ since E_n/R^* has an asymptotic value of $-\bar{V}_0$. Figures 10(a) and 10(b) show the oscillator strength as a function of $\bar{V}_0$ and $\bar{\zeta}$, respectively. From these it is seen that f_0^a increases according to $f_0^a\propto\bar{V}_0^{1/4}$ as $\bar{V}_0\to\infty$ for a fixed value of $\bar{\zeta}$. In the limit of $\bar{\zeta}\to\infty$ with a fixed value of $\bar{V}_0$, on the other hand, f_0^a approaches zero as $f_0^a\propto\bar{\zeta}^{-1/2}$. Also, in another limit of $\bar{\zeta}\to0$, f_0^a vanishes. Therefore, there is an optimal potential width to make the oscillator strength maximum for a fixed value of $\bar{V}_0$.

V. DISCUSSION

A. Comparison with three- and two-dimensional cases

To facilitate the following discussion, results of the three- and two-dimensional cases are briefly reviewed here. In the isotropic bulk (3D) system,[11] the Sommerfeld factors for allowed and forbidden transitions were obtained as

$$S_a^{3D}=\frac{\pi\alpha_3 e^{\pi\alpha_3}}{\sinh(\pi\alpha_3)}\ , \tag{5.1a}$$

$$S_f^{3D}=(1+\alpha_3^2)\frac{\pi\alpha_3 e^{\pi\alpha_3}}{\sinh(\pi\alpha_3)}\ , \tag{5.1b}$$

respectively, where $\alpha_3=(R^*)^{1/2}(\hbar\omega-E_g^{\text{bulk}})^{-1/2}$. These are always *larger than unity,* indicating that the Coulomb attraction between an electron and a hole *enhances* the optical absorption for both allowed and forbidden transitions. This also holds for the two-dimensional system,[12] where the Sommerfeld factors given by

$$S_a^{2D}=\frac{e^{\pi\alpha_2}}{\cosh(\pi\alpha_2)}\ , \tag{5.2a}$$

$$S_f^{2D}=(1+4\alpha_2^2)\frac{e^{\pi\alpha_2}}{\cosh(\pi\alpha_2)}\ , \tag{5.2b}$$

are larger than unity. Here $\alpha_2=(R^*)^{1/2}(\hbar\omega-E_g^{2D})^{-1/2}$. This is why the Sommerfeld factor has also been called

the "Coulomb *enhancement* factor." In these two cases, there is no divergence difficulty even if the attraction between an electron and a hole is given by the *bare* Coulomb interaction.

On the other hand, the bare Coulomb attraction induces some anomalous features in the 1D case. As seen in Fig. 2, the Coulomb interaction between an electron and a hole *suppresses* the allowed interband absorption intensity. Moreover, the allowed interband absorption vanishes completely in the case of the bare Coulomb attraction which corresponds to the zero cutoff, i.e., $z_0=0$. These anomalous results can be understood qualitatively by considering the absorption due to discrete exciton states below E_g. As pointed out in Sec. IV, for the case of long-range interaction between an electron and a hole, the oscillator strength of the lowest exciton state becomes very large and almost the entire oscillator strength concentrates on this bound state. Then, as a consequence of the f-sum rule, the oscillator strength of the interband transition becomes very weak.[16] This is a remarkable feature of the purely one-dimensional system, in striking contrast to the 3D and 2D systems. The same situation holds also for the case of short-range interaction. Moreover, as can be seen in Fig. 1, a small amplitude of the unbound gerade-parity wave function at the origin, which results in the suppressed interband absorption for the case of an allowed transition, is accompanied by a large derivative of the ungerade-parity wave function at the origin. Therefore, the interband absorption for the forbidden transition becomes stronger in the opposite way as the absorption intensity for the allowed transition decreases. Thus the Sommerfeld factor S_f for the forbidden transition increases as the electron-hole attraction becomes stronger. This also holds for the case of short-range interaction.

Another remarkable feature of the 1D system appears in the eigenenergy series[17] of the bound states. The energies of the bound states with the s-wave symmetry in the 3D and 2D cases are exactly evaluated as

$$E_n^{3D}=-\frac{R^*}{(n+1)^2}\ , \tag{5.3a}$$

$$E_n^{2D}=-\frac{R^*}{(n+\frac{1}{2})^2}\ , \tag{5.3b}$$

where $n=0,1,2,\ldots$ and $n=0$ stands for the lowest-energy exciton state. Thus the binding energy of the lowest exciton is finite for both 3D and 2D cases even if the electron-hole attractive potential is the bare Coulomb potential. On the other hand, in the case of the 1D bare Coulomb potential, the binding energy of the lowest exciton state is infinitely large as shown in Sec. IV. These features suggest that the attractive force between an electron and a hole in the 1D system is more effective than in the 3D and 2D systems. Intuitively speaking, in the 3D and 2D systems, a particle can move around the origin of the Coulomb potential without directly touching the origin. On the other hand, in the 1D system, a particle is always moving through the origin because the spatial direction of motion is restricted to one dimension. Thus the particle motion in the 1D system is affected by the infinitely deep potential at the origin more strongly than in the 3D and 2D systems. In mathematical terms this situation can be understood as follows. The spatial phase volume around the origin is given as $4\pi r^2 dr$, $2\pi r dr$, and $2dr$ for 3D, 2D, and 1D systems, respectively, where spherical, circular, and linear shell regions from r to $r+dr$ are considered. Then the $1/r$ singularity of the Coulomb potential is removed upon integration around the origin for the 3D and 2D cases, whereas a logarithmic singularity remains for the 1D case. Thus the energy and wave function of the excitonic state in the 1D system are sensitively dependent on the potential profile near the

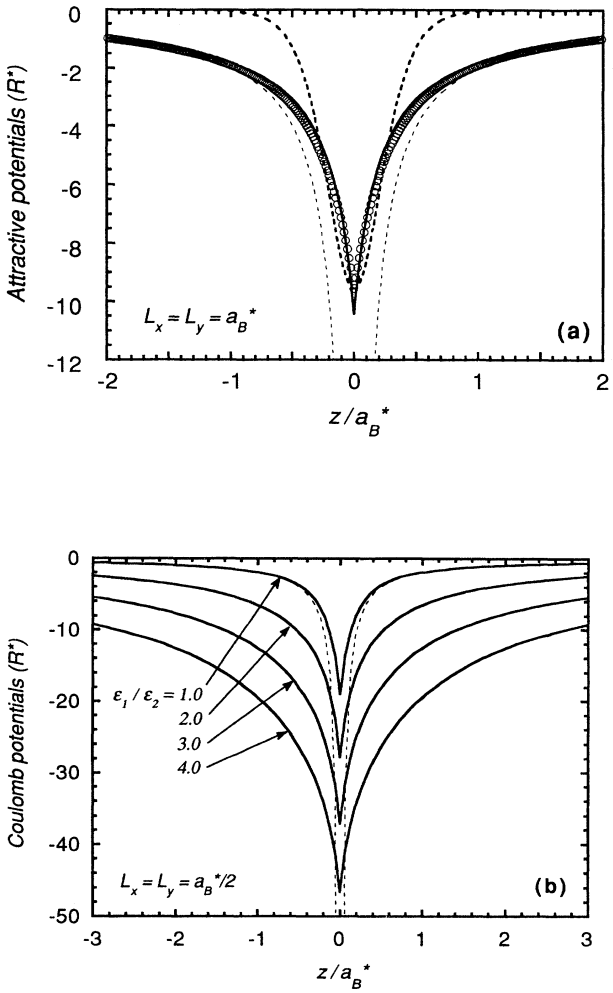

FIG. 11. (a) Several attractive potentials are compared. The bare Coulomb potential corresponds to the thin dotted curve, the cutoff Coulomb potential given by Eq. (2.8a) to the thick solid curve, and the short-range potential given by Eq. (2.8c) to the thick dashed curve. The parameters employed are $z_0/a_B^*=0.19$, $\zeta/a_B^*=0.22$, and $V_0/R^*=9.55$. Open circles describe the effective 1D Coulomb potential without the dielectric effect for $L_x=L_y=a_B^*$. (b) The effective 1D Coulomb potentials given by Eq. (5.7), which include the dielectric effect are plotted for a wire having the lateral size of $L_x=L_y=\frac{1}{2}a_B^*$ and for $\epsilon_1/\epsilon_2=1.0$, 2.0, 3.0, and 4.0 from top to bottom. The thin dotted curve represents the bare Coulomb potential for $\epsilon_1/\epsilon_2=1.0$.

origin. This feature explains also the qualitatively similar behaviors of the Sommerfeld factors in the 1D system for both cases of the long- and short-range interactions, because the major difference between these two potentials appears only in the long-distance region.

B. Feasibility of the model potentials

Now we shall discuss the feasibility of the modified Coulomb potential with a cusp-type cutoff given in Eq. (2.8a). Several types of cutoff have been introduced, initially only to avoid the difficulty of divergence and to make the problem analytically solvable.[4-6] Among them, the potential of Eq. (2.8a) is the most effective and useful one in discussing the optical properties of a semiconductor wire. The reason will be given in this subsection.

The effective 1D Coulomb potential between an electron and a hole was derived in Sec. II, taking into account the subband quantization in the lateral directions. In the strong confinement regime, this effective potential is given by Eq. (2.7). The effective 1D Coulomb potential was estimated in a similar way for cylindrical and square semiconductor wires.[18] A more general expression of the effective potential including a dielectric effect is given in the next subsection [Eq. (5.7)]. When an electron and a hole are confined in a square wire whose lateral size is specified by L_x and L_y, the lowest subband function is given as

$$f^0(x,y)=\frac{2}{\sqrt{L_xL_y}}\cos\left[\frac{\pi x}{L_x}\right]\cos\left[\frac{\pi y}{L_y}\right], \tag{5.4}$$

for $|x|\le\frac{1}{2}L_x$ and $|y|\le\frac{1}{2}L_y$. The effective 1D potential calculated by Eq. (2.7) using Eq. (5.4) is shown in Fig. 11(a) for the case of $L_x=L_y=a_B^*$. The results plotted by open circles can be fitted very well by Eq. (2.8a), which is shown by a solid curve. The cutoff z_0 is found to be proportional to the lateral size of the wire. Thus the cusp-type Coulomb potential has the simplest form enabling analytical solutions and also describes rather well the actual potential in the quantum-wire structures.

Our formulation is concerned only with the *linear* optical properties under weak excitation. In the strong excitation regime, on the other hand, several many-body effects would appear and induce interesting optical nonlinearities. Among them, the screening effect on the electron-hole attractive interaction in the 1D system is not yet clarified satisfactorily. Although the shape of the screened potential in the 1D system is not known precisely, the model potential Eq. (2.8c) can be expected to describe the screening effect qualitatively.

C. Dielectric effect

In determining the effective 1D Coulomb potential between an electron and a hole, we have averaged the bare 3D Coulomb potential, taking into account the motion of the particles in the confining directions (x and y). Here we shall include also the dielectric effect arising from the difference in the dielectric constant between the quantum wire and the surrounding material.

Extending the image-charge method developed for the case of quantum wells,[19] the interaction between an electron at a position $\mathbf{r}_e=(x_e,y_e,z_e)$ and a hole at $\mathbf{r}_h=(x_h,y_h,z_h)$ in a wire ($|x|\le\frac{1}{2}L_x$, $|y|\le\frac{1}{2}L_y$) including the dielectric effect is derived as

$$U(\mathbf{r}_e,\mathbf{r}_h)=-\frac{e^2}{\epsilon_1}\sum_{m=-\infty}^{\infty}\sum_{n=-\infty}^{\infty}\frac{\delta^{|m|+|n|}}{[(x_h-x_e^m)^2+(y_h-y_e^n)^2+(z_h-z_e)^2]^{1/2}}, \tag{5.5}$$

with

$$\delta=\frac{\epsilon_1-\epsilon_2}{\epsilon_1+\epsilon_2}, \tag{5.6}$$

where ϵ_1 (ϵ_2) is the dielectric constant of the quantum wire (surrounding medium), $x_e^m=mL_x+(-1)^m x_e$, and $y_e^n=nL_y+(-1)^n y_e$. After averaging over x_e, y_e, x_h, and y_h with a weight $|f_e^0(x_e,y_e)|^2|f_h^0(x_h,y_h)|^2$ associated with the lowest subband state given in Eq. (5.4), we have

$$V_{\rm eff}^{\rm 1D}(|z_e-z_h|)=-\frac{4R^*}{\bar{L}_x\bar{L}_y}\int_0^\infty dk_x\int_0^\infty dk_y F(k_x)F(k_y)\exp\left\{-\pi|\bar{z}_e-\bar{z}_h|\left[\left[\frac{k_x}{\bar{L}_x}\right]^2+\left[\frac{k_y}{\bar{L}_y}\right]^2\right]^{1/2}\right\}\left[\left[\frac{k_x}{\bar{L}_x}\right]^2+\left[\frac{k_y}{\bar{L}_y}\right]^2\right]^{-1/2}, \tag{5.7}$$

where the overbar means the scaling by the effective Bohr radius a_B^* and

$$F(k)=\frac{1-\delta^4+2\delta(1-\delta^2)\cos(\pi k)}{1-2\delta^2\cos(2\pi k)+\delta^4}G(k). \tag{5.8}$$

Here $G(k)$ is given using the spherical Bessel function of the zeroth-order $j_0(x)=\sin x/x$ as

$$G(k)=j_0^2\left[\frac{\pi}{2}k\right]+j_0\left[\frac{\pi}{2}(k-2)\right]j_0\left[\frac{\pi}{2}k\right]+j_0\left[\frac{\pi}{2}(k+2)\right]j_0\left[\frac{\pi}{2}k\right]$$
$$+\frac{1}{4}j_0^2\left[\frac{\pi}{2}(k-2)\right]+\frac{1}{4}j_0^2\left[\frac{\pi}{2}(k+2)\right]+\frac{1}{2}j_0\left[\frac{\pi}{2}(k-2)\right]j_0\left[\frac{\pi}{2}(k+2)\right]. \quad (5.9)$$

Numerical results are plotted in Fig. 11(b) for various values of $\epsilon_1/\epsilon_2 \geq 1$. In this case also, the potential can be well fitted by Eq. (2.8a), although in the limit of $|z|\to\infty$, the potential approaches the Coulomb potential given by $-(\epsilon_1/\epsilon_2^2)e^2/|z|$. As the ratio ϵ_1/ϵ_2 increases, the attractive potential becomes more long ranged and is enhanced for all regions of z over the bare Coulomb potential $-e^2/\epsilon_1|z|$ depicted by a dashed curve. Therefore, the peculiar features of the Sommerfeld factor described in Sec. III would be more pronounced by the dielectric effect.

D. Experimental observability

We would like to comment on the possibility of experimental observation of the peculiar features of the Sommerfeld factor. A primary requirement for observation is that the intersubband spacing is much larger than the exciton binding energy so that the continuum exciton states associated with the lowest subband do not overlap with the discrete exciton states associated with the higher subbands. Assuming a square-wire structure and the complete confinement of carriers, we can estimate the energy separation between the lowest subband and higher one as $8\pi^2(a_B^*)^2/L^2$ in units of R^*. This separation should be much larger than the exciton binding energy to justify the 1D treatment of the wire. Roughly speaking, only *when the lateral size of the wire is smaller than the bulk exciton Bohr radius,* not only does the center-of-mass motion show a one-dimensional nature, but also the electron-hole relative motion of the exciton in the wire. For example, L_x and L_y should be less than 100 Å for GaAs to justify the 1D treatment. Otherwise, the confinement in the lateral directions becomes weak and the electron-hole relative motion is not necessarily one dimensional even though the center-of-mass motion shows a 1D character, so that the peculiar features due to the 1D nature of the electron-hole relative motion would not be clearly seen in optical spectra.

Another feature to be considered in observing the peculiar characteristics of the Sommerfeld factor is the finiteness of the potential barrier height, which weakens the one dimensionality of the electron-hole relative motion and obscures the spectral features. It is also important to consider various line-broadening effects due to scattering by the interface roughness and phonons which also smear the spectral characteristics. However, we did not go into details of these problems and leave them for future study.

For an allowed transition, the weak interband absorption and the absence of the van Hove singularity are remarkable results in this paper. However, these lead to difficulty in identifying the band edge in the absorption spectra. In order to determine the band edge, the two-photon absorption and electroabsorption experiments would be useful because the selection rules in these experiments are complementary to those in the one-photon absorption and the information about the exciton states which are not accessible by the linear absorption can be obtained. Combining the knowledge on the energy positions of exciton states of the even and odd parities and analyzing the data by an appropriate theoretical model, we can eventually determine the band edge.

For observing the peculiar features of the 1D system in optical-absorption spectra clarified in this paper, not only inorganic semiconductor wires, but also organic semiconducting chains, which can be called "natural quantum wires," e.g., organo polysilanes (Si polymers), and polydiacetylenes are good candidates. In fact, both exhibit very strong exciton absorption below the band edge and weak interband absorption.[20] In their absorption spectra, the van Hove singularity of the 1D system is completely absent. These results seem to coincide with our results. In addition, only a few absorption lines due to 1D excitons are observed. This may suggest that the electron-hole interaction in this system is short range because the number of bound states is finite in the case of short-range interaction as shown in Sec. IV. However, it is too premature to conclude that our theory can successfully explain the experimental results because the electron-lattice coupling in the organic low-dimensional system is thought to be stronger than in the inorganic systems. Interchain interactions are also to be investigated which might have an effect on the cutoff z_0 through the 3D character of the wave function. Comprehensive understanding is left for future studies.

Finally, we would like to suggest a very interesting optical nonlinearity arising from the suppressed interband absorption in the 1D system. There is a possibility of realizing an "increasing absorption" in the pump-probe measurement of semiconductor wires with a direct allowed transition. When the excitation is rather strong, the attractive interaction between an electron and a hole becomes weaker because of the screening effect. Then the absorption intensity of the discrete exciton states decreases and consequently the interband absorption increases. Therefore, the absorption intensity above the band edge just after pumping is larger than that before pumping. The remarkable feature of this system is that the increasing absorption can be realized by an *intrinsic*

mechanism in contrast to self-electro-optic-effect devices[21] in which an external electric field is used.

VI. CONCLUSIONS

Modeling a semiconductor quantum wire as a purely 1D system and employing some model potentials between an electron and a hole, which describe a modified Coulomb interaction and a short-range interaction, we have calculated analytically the wave function, eigenenergy, and oscillator strength of the bound and unbound exciton states in the 1D system. Using these results, the linear optical-absorption spectra of the 1D system have been obtained analytically for both allowed and forbidden direct transitions. The Sommerfeld factor is smaller than unity for an allowed interband transition, in striking contrast to the 3D and 2D cases. This peculiar feature can be understood in terms of the anomalously strong concentration of the oscillator strength on the lowest-energy exciton state. On the other hand, for the direct forbidden transition, the Sommerfeld factor is larger than unity and behaves similarly to the 3D and 2D cases. These properties hold irrespective of the interaction range of the electron-hole attractive potential. Finally, the Coulomb potential with a cusp-type cutoff describes fairly well an effective 1D potential in an actual semiconductor wire with a finite cross section. This correspondence would be valid only when the lateral size of the wire is smaller than the exciton Bohr radius. The dielectric effect in the wire was also investigated and found to lead to the enhancement of the peculiar features of the 1D system.

Although our models do not include all the actual details, e.g., the electron-lattice interaction and line-broadening effect, we believe that these new findings hold quite universally in a 1D system and will be of great significance in the interpretation of experimental results. In this sense, as far as inorganic semiconductor wires are concerned, our model calculations may serve as a standard model for the linear optical properties of the quantum wire.

ACKNOWLEDGMENTS

The authors would like to thank Dr. H. Kanbe, Dr. T. Fukui, Dr. N. Matsumoto, and Dr. N. Uesugi for their helpful discussions and Dr. Y. Horikoshi and Dr. T. Kimura for their encouragement. Dr. H. Ando is also acknowledged for his fruitful comments on an effective Coulomb potential in a quantum wire. One of the authors (T.O.) thanks Dr. A. Shimizu (Quantum Wave Project, JRDC) and Professor H. Sakaki (the University of Tokyo) for their fruitful comments in stimulating discussions.

APPENDIX A: CALCULATION OF NORMALIZATION CONSTANTS OF THE UNBOUND WAVE FUNCTIONS

In the case of long-range interaction, the gerade and ungerade wave functions have the forms of

$$\phi_k^g(z)=N_g^{\rm long}[D_0^{(2)}W^{(1)}(x)-D_0^{(1)}W^{(2)}(x)]\ , \tag{A1a}$$

$$\phi_k^u(z)=N_u^{\rm long}[W_0^{(2)}W^{(1)}(x)-W_0^{(1)}W^{(2)}(x)]\ , \tag{A1b}$$

respectively, where $N_g^{\rm long}$ and $N_u^{\rm long}$ are normalization constants to be determined. The asymptotic form of the wave function can be obtained with the use of

$$W^{(1)}_{-i\alpha,1/2}(x)\sim|x|^{i\alpha}\exp(-\alpha\theta+\tfrac{1}{2}|x|e^{i\theta})\ ,$$
$$=e^{-\pi\alpha/2}e^{ikz_0}[2k(|z|+z_0)]^{i\alpha}e^{ik|z|}\ , \tag{A2a}$$

$$W^{(2)}_{-i\alpha,1/2}(x)\sim-e^{-\pi\alpha}|x|^{-i\alpha}\exp(\alpha\theta-\tfrac{1}{2}|x|e^{i\theta})\ ,$$
$$=-e^{-\pi\alpha/2}e^{-ikz_0}[2k(|z|+z_0)]^{-i\alpha}e^{-ik|z|}\ , \tag{A2b}$$

where $\theta=\arg x=\pi/2$ and $\alpha=(a_B^* k)^{-1}$. The probability current is defined as

$$j_\pm\equiv\frac{i\hbar}{2\mu}\left[\phi_k^\pm\frac{d}{dz}(\phi_k^\pm)^*-(\phi_k^\pm)^*\frac{d}{dz}\phi_k^\pm\right]\ , \tag{A3}$$

where ϕ_k^+ (ϕ_k^-) is a right- (left-) travelling component of an unbound wave function. This is evaluated in the asymptotic region of $|z|\to\infty$ as

$$|j_+^g|=\frac{\hbar k}{\mu}(N_g^{\rm long})^2e^{-\pi\alpha}|D_0^{(2)}|^2\ , \tag{A4a}$$

$$|j_-^g|=\frac{\hbar k}{\mu}(N_g^{\rm long})^2e^{-\pi\alpha}|D_0^{(1)}|^2\ , \tag{A4b}$$

$$|j_+^u|=\frac{\hbar k}{\mu}(N_u^{\rm long})^2e^{-\pi\alpha}|W_0^{(2)}|^2\ , \tag{A4c}$$

$$|j_-^u|=\frac{\hbar k}{\mu}(N_u^{\rm long})^2e^{-\pi\alpha}|W_0^{(1)}|^2\ . \tag{A4d}$$

The k-scale normalization can be done with the aid of the relation[14]

$$|j_+|+|j_-|\equiv\frac{1}{2\pi}\frac{\hbar k}{\mu}\ . \tag{A5}$$

Then the normalization constants are determined as

$$N_g^{\rm long}=\left[\frac{e^{\pi\alpha}}{2\pi}\right]^{1/2}(|D_0^{(1)}|^2+|D_0^{(2)}|^2)^{-1/2}\ , \tag{A6a}$$

$$N_u^{\rm long}=\left[\frac{e^{\pi\alpha}}{2\pi}\right]^{1/2}(|W_0^{(1)}|^2+|W_0^{(2)}|^2)^{-1/2}\ . \tag{A6b}$$

On the other hand, the wave functions in the case of short-range interaction can be written as

$$\phi_k^g(z)=N_g^{\rm short}[g_k'(0)f_k(\xi)-f_k'(0)g_k(\xi)]\ , \tag{A7a}$$

$$\phi_k^u(z)=N_u^{\rm short}[g_k(0)f_k(\xi)-f_k(0)g_k(\xi)]\ , \tag{A7b}$$

for gerade and ungerade parities, respectively. Using the relation Eq. (A5) and asymptotic expressions in the limit of $z\to\infty$ ($\xi\to1$) given as

$$f_k(\xi)\sim2^{-ik\xi}e^{ikz}\ , \tag{A8a}$$

$$g_k(\xi)\sim2^{-ik\xi}e^{-ikz}\ , \tag{A8b}$$

we can determine the normalization constants in a similar manner to the long-range case as

$$N_g^{\text{short}}=\frac{1}{\sqrt{2\pi}}[|f_k'(0)|^2+|g_k'(0)|^2]^{-1/2}\ , \tag{A9a}$$

$$N_u^{\text{short}}=\frac{1}{\sqrt{2\pi}}[|f_k(0)|^2+|g_k(0)|^2]^{-1/2}\ . \tag{A9b}$$

APPENDIX B: DIVERGENCE OF SPECTRA NEAR THE BAND EDGE IN THE CASE OF SHORT-RANGE INTERACTION

The mathematical origin of the divergence of the absorption spectra in the case of the short-range interaction is briefly shown in this appendix. Near the band edge, i.e., $k\to 0$ the hypergeometric functions $f_k(0)$ and $g_k(0)$ defined in Eq. (3.28) have the following forms:

$$f_0(0)=g_0(0)=\sqrt{\pi}\left[\Gamma\left[\frac{1-s}{2}\right]\Gamma\left[\frac{2+s}{2}\right]\right]^{-1}\ , \tag{B1a}$$

$$f_0'(0)=g_0'(0)=\frac{s(s+1)\sqrt{\pi}}{2}\left[\Gamma\left[\frac{2-s}{2}\right]\Gamma\left[\frac{3+s}{2}\right]\right]^{-1}\ , \tag{B1b}$$

resulting in $|g_k'(0)f_k(0)-f_k'(0)g_k(0)|\to 0$ as $k\to 0$. When we expand $|g_k'(0)f_k(0)-f_k'(0)g_k(0)|$ around $k=0$ as

$$|g_k'(0)f_k(0)-f_k'(0)g_k(0)|\sim\beta(s)k\ , \tag{B2}$$

the absorption coefficient, and the Sommerfeld factors near the band edge are asymptotically given as

$$K_a^{\text{short}}(\hbar\omega\sim E_g)\sim\frac{\beta^2(s)k}{s^2(s+1)^2}\left[\Gamma\left[\frac{2-s}{2}\right]\Gamma\left[\frac{3+s}{2}\right]\right]^2\ , \tag{B3a}$$

$$S_a^{\text{short}}(\hbar\omega\sim E_g)\sim\frac{\beta^2(s)k^2}{s^2(s+1)^2}\left[\Gamma\left[\frac{2-s}{2}\right]\Gamma\left[\frac{3+s}{2}\right]\right]^2\ , \tag{B3b}$$

$$K_f^{\text{short}}(\hbar\omega\sim E_g)\sim\beta^2(s)k\left[\Gamma\left[\frac{1-s}{2}\right]\Gamma\left[\frac{2+s}{2}\right]\right]^2\ , \tag{B3c}$$

$$S_f^{\text{short}}(\hbar\omega\sim E_g)\sim\beta^2(s)\left[\Gamma\left[\frac{1-s}{2}\right]\Gamma\left[\frac{2+s}{2}\right]\right]^2\ . \tag{B3d}$$

Then K_a^{short} (K_f^{short}) diverges for $s=2,4,6,\ldots$ ($s=1,3,5,\ldots$) through the divergence of the Γ function whose argument is a negative integer. The exact expression of $\beta(s)$ is rather complicated and is not shown here.

---

[1]M. Tsuchiya, J. M. Gaines, R. H. Yan, R. J. Simes, P. O. Holts, L. A. Coldren, and P. M. Petroff, Phys. Rev. Lett. **62**, 466 (1989); D. Gershoni, J. S. Weiner, S. N. G. Chu, G. A. Baraff, J. M. Vanderberg, L. N. Pfeiffer, K. West, R. A. Logan, and T. Tanbun-Ek, *ibid.* **65**, 1631 (1990); M. Tanaka and H. Sakaki, Appl. Phys. Lett. **54**, 1326 (1989); H. Kanbe, A. Chavez-Pirson, H. Ando, H. Saito, and T. Fukui, *ibid.* **58**, 2969 (1991).

[2]E. Kapon, D. M. Hwang, and R. Bhat, Phys. Rev. Lett. **63**, 430 (1989).

[3]T. Ogawa and T. Takagahara, Phys. Rev. B **43**, 14 325 (1991); Surf. Sci. (to be published).

[4]R. Loudon, Am. J. Phys. **27**, 649 (1959).

[5]R. J. Elliott and R. Loudon, J. Phys. Chem. Solids **8**, 382 (1959); **15**, 196 (1960).

[6]S. Abe, J. Phys. Soc. Jpn. **58**, 62 (1989).

[7]Applying the WKB approximation and Bohr-Sommerfeld quantization rule to the 1D bare Coulomb problem leads to erroneous results. For example, the binding energy of the lowest exciton state becomes *finite* and is 4 times that in the 2D case. Namely, the eigenenergy of the bound state is incorrectly given as $E_n^{\text{1D,WKB}}=-4R^*/(n+\frac{1}{2})^2$ for $n=0,1,2,\ldots$.

[8]In this paper we use the term "one-dimensional exciton" for an exciton whose electron-hole *relative motion* is described by a 1D wave function. The center-of-mass motion is, of course, one dimensional.

[9]In calculating the normalization constant of an unbound wave function, the n_0-scale normalization has been employed in the literature, e.g., Refs. 10 and 12, where n_0 is the number of states within a phase volume of length k in the k space. In the one-dimensional system, n_0 is proportional to k. Therefore, the k-scale normalization coincides with the n_0-scale version.

[10]H. A. Bethe and E. E. Salpeter, *Quantum Mechanics of One- and Two-Electron Atoms* (Springer-Verlag, Berlin, 1957), p. 22.

[11]R. J. Elliott, Phys. Rev. **108**, 1384 (1957).

[12]M. Shinada and S. Sugano, J. Phys. Soc. Jpn. **21**, 1936 (1966).

[13]The band-gap energy E_g is implicitly assumed to be much larger than the energy considered here, e.g., the exciton binding energy, so as to make the effective-mass approximation valid. Therefore, the factor $w+\bar{E}_g$ in, e.g., the numerators of Eqs. (3.12) and (3.14) can be regarded as almost a constant.

[14]L. D. Landau and E. M. Lifshitz, *Quantum Mechanics,* 3rd ed. (Pergamon, Oxford, 1977).

[15]Strictly speaking, the nth state in the case of $s=n$ is an *unbound* state because the wave function is completely delocalized.

[16]The f-sum rule does not hold precisely here because we employ the effective-mass approximation which is valid only in the energy region near the band edge. However, the f-sum rule is useful for qualitative understanding.

[17]T. Nakayama (private communication). The Schrödinger equation in a d-dimensional space ($d=1,2,3,4,\ldots$) with the bare Coulomb potential has been analytically solved and then the eigenenergy of the bound states is given for the d-dimensional case as $E_n^{d\,\text{D}}=-R^*[n+(d-1)/2]^{-2}$ for

$n=0,1,2,\ldots$.

[18]L. Bányai, I. Galbraith, C. Ell, and H. Haug, Phys. Rev. B **36**, 6099 (1987); H. Ando, H. Oohashi, and H. Kanbe, J. Appl. Phys. (to be published).

[19]M. Kumagai and T. Takagahara, Phys. Rev. B **40**, 12 359 (1989).

[20]P. Trefonas, R. West, R. D. Miller, and D. Hofer, J. Polym. Sci. Polym. Lett. Ed. **21**, 823 (1983); H. Tachibana, Y. Kawabata, S. Koshihara, and Y. Tokura, Solid State Commun. **75**, 5 (1990).

[21]D. A. B. Miller, D. S. Chemla, T. C. Damen, A. C. Gossard, W. Wiegmann, T. H. Wood, and C. A. Burrus, Appl. Phys. Lett. **45**, 13 (1984).